NUMERICAL MODELING OF THE FILTER SAND PERFORMANCE IN EMBANKMENT DAM UNDER STATIC AND DYNAMIC CONDITIONS

A Thesis Submitted to
the Graduate School of
İzmir Institute of Technology
in Partial Fulfillment of the Requirements for Degree of

MASTER OF SCIENCE

in Civil Engineering

by
Aybüke KARAOĞLU

June 2023
İZMİR

We approve the thesis of **Aybüke KARAOĞLU**

Examining Committee Members:

Prof. Dr. Nurhan ECEMİŞ
Department of Civil Engineering, İzmir Institute of Technology

Prof. Dr. Alper SEZER
Department of Civil Engineering, Ege University

Asst. Prof. Volkan İŞBUĞA
Department of Civil Engineering, İzmir Institute of Technology

22 June 2023

Prof. Dr. Nurhan ECEMİŞ
Supervisor, Department of Civil Engineering, İzmir Institute of Technology

Prof. Dr. Cemalettin DÖNMEZ
Head of the Department of Civil Engineering

Prof. Dr. Mehtap EANES
Dean of the Graduate School

ACKNOWLEDGMENTS

This thesis study dedicated to the people who affected by the Kahramanmaraş Earthquakes in February, 2023.

First and foremost, my deep and sincere gratitude is given to my supervisor, Prof. Dr. Nurhan Ecemiş for her support, guadiance and patience throughout this study. Second, I would like to thank Hadi Valizadeh for his effort in the laboratory and all the data he collected that I used in my study.

I would like to thank my thesis examining committee members, Prof. Dr. Alper Sezer and Asst. Prof. Volkan İşbuğa for their precious comments on my thesis.

I also would like to thank Dr. Mustafa Koç and Başak Karsavuran for sharing their experiences. My heartfelt thanks go to Merve Budak who we felt the same way during the study and finished the journey together.

My special thanks to my parents, Emine and Fethi, my brother and my sister-in-law, Abdurrahman and Şengül for their caring and unconditional support in my whole life. Thanks to my nephews Kuzey Arslan and Ateş, the joy is always in the family.

My final thanks go to Emir Aybars Dizman who is always there for me with all happy and hard moments.

ABSTRACT

NUMERICAL MODELING OF THE FILTER SAND PERFORMANCE IN EMBANKMENT DAM UNDER STATIC AND DYNAMIC CONDITIONS

The filter material in embankment dams is a crucial part of the dam due to protecting the core material (usually clay) against internal erosion. Internal erosion is defined as the transportation of core material particles to the filter material by seepage flow. It is the main reason for the deformation and loss of resistance in the body and foundation of a dam. Therefore, it is a serious threat risk to embankment dams. To prevent internal erosion, it is necessary to accurately evaluate the interaction between water-filter material-core material during the dam's design and operation stages. A suitable filter material should be able to control and block cracks that can form in the core material. Terzaghi (1925) did the first research on filter material and proposed a criterion based on the particle size of a clay. Another detailed study was conducted by Sherard et al. (1989) who developed an experiment called No Erosion Filter Test (NEF Test) to comprehend the relationship between filter and core materials. NEF Test is seen as the most proper method to determine the critical filter which leans on the impermeable core material in the downstream side of an embankment dam. In the NEF test, the most severe condition that can occur is represented as an erosive leak from the core material to the filter material.

Within the scope of this study, the internal erosion of the backfill used in the dam is studied through outflow rate and deformations in the base sample (clay). First, the samples taken from two embankment dams in Izmir (Kalabak Dam and Rahman Dam) were brought to the geotechnical laboratory of Izmir Institute of Technology (IZTECH), and the filter material was mixed with fine materials (silt) in different contents. A series of NEF Tests were performed in the IZTECH-geotechnical laboratory on the filter and core samples of Kalabak Dam within a TUBITAK Project No. 221M071 (Ecemis, 2023). Then, the performed NEF Tests were modeled by the finite difference method (FDM) using the Itasca-FLAC3D software. Finally, the outcomes of the numerical models were compared to experimental results. Numerical models had a good agreement to decide whether filter sand performance is successful or not.

ÖZET

DOLGU BARAJLARDAKİ FİLTRE KUMUNUN PERFORMANSININ STATİK VE DİNAMİK YÜKLEME KOŞULLARI ALTINDA NÜMERİK MODELLENMESİ

Toprak dolgu barajlarda, filtre malzemesi, çekirdeği (genellikle kil) erozyona karşı koruma işlevinden dolayı oldukça önemlidir. Çekirdek içerisindeki ince daneli malzemelerin sızıntı (iç akış) sebebiyle filtre malzemesine taşınması süreci içsel erozyon olarak tanımlanır. İçsel erozyon, dolgu barajların gövdesinde veya temelinde meydana gelen mukavemet kaybının veya deformasyonların ana sebebidir. Dolayısıyla içsel erozyon dolgu barajlar için ciddi bir tehdit unsurudur. İçsel erozyonun önüne geçebilmek için tasarım ve yapım aşamalarında su-filtre-çekirdek etkileşiminin doğru değerlendirilmesi gerekir. Uygun bir filtre malzemesi, geçirgen olmayan çekirdek kısmında oluşabilecek çatlakları kontrol edebilme ve engelleme özelliğine sahip olmalıdır. Filtre malzemesine yönelik ilk çalışma Terzaghi tarafından yapılmıştır ve filtre malzemesi için kil çapına bağlı bir tasarım kriteri önermiştir (1925). Filtre malzemesi üzerindeki diğer bir detaylı araştırma ise Sherard vd. (1989) tarafından yapılmıştır. Araştırmacılar filtre-çekirdek malzeme ilişkisini değerlendirmek için laboratuvarda Erozyonsuz Filtre Deneyi (No Erosion Filter Test, NEF Test) geliştirmiştir.

NEF Testi, bir toprak dolgu barajın mansap tarafında geçirimsiz çekirdek malzemeye yaslanan kritik filtreyi belirlemek için en uygun yöntem olarak görülmektedir. Testte, oluşabilecek en riskli durum, çekirdek malzemeden filtre malzemesine erozif bir sızıntı olarak temsil edilmektedir. İzmir'deki iki toprak dolgu barajından (Kalabak Barajı ve Rahman Barajı) alınan numuneler laboratuvara getirilmiş ve filtre malzemesi farklı içeriklerde ince malzemelerle karıştırılmıştır. Bu çalışma kapsamında, İzmir Yüksek Teknoloji Enstitüsü laboratuvarında Kalabak Barajı'nın filtre ve çekirdek numuneleri üzerinde gerçekleştirilen NEF Deneyleri serisi FLAC3D yazılımı kullanılarak modellenmiştir. İçsel erozyon, çıkış hızı ve taban numunesindeki deformasyonlar aracılığıyla doğrulanarak filtre kumunun performansı değerlendirilmiştir.

TABLE OF CONTENTS

LIST OF FIGURES viii

LIST OF TABLES xi

LIST OF SYMBOLS AND ABBREVIATIONS xii

CHAPTER 1. INTRODUCTION 1
1.1. General 1
1.2. Motivation of the Thesis 3
1.3. Organization of the Thesis 5

CHAPTER 2. LITERATURE REVIEW OF INTERNAL EROSION 6
2.1. Introduction 6
2.2. Internal Erosion Phenomena in Embankment Dams 6
2.3. Filter Design Criteria 9
2.4. No Erosion Filter (NEF) Test 13
2.5. Conclusion 15

CHAPTER 3. NO EROSION FILTER (NEF) TEST 16
3.1. Introduction 16
3.2. Test Setup 17
3.2.1. NEF Test Apparatus 17
3.2.2. Base and Filter Materials Used in the NEF Tests 19
3.3. Static Tests 22
3.3.1. Static Test without Fine Particles (FC = 0%) 22
3.3.2. Static Test for Fines Content of 2% 24
3.3.3. Static Test for Fines Content of 5% 26
3.4. Dynamic Tests 28
3.4.1. Dynamic Test for 2Hz Frequency 30
3.4.2. Dynamic Test for 4Hz Frequency 32
3.5. Summary of NEF Tests 35

CHAPTER 4. NUMERICAL MODELING OF INTERNAL EROSION 38
4.1. Introduction 38
4.2. Numerical Modeling of Internal Erosion 38
4.3. FLAC 3D 40
4.3.1. Fluid-Mechanical Interaction in FLAC3D 40
4.4. NEF Test Modeling 41
4.4.1. Model Geometry 41
4.4.2. Initial and Boundary Conditions 43
4.4.3. Material Used in the Models 43
4.4.4. Dynamic Loading 47
4.5. Results of Static Numerical Models 47
4.5.1. Numerical Model Results of Static Test without Fine Particles in the Filter 48
4.5.2. Numerical Model Results of Static Test with 2% Fines Content in the Filter 50
4.5.3. Numerical Model Results of Static Test with 5% Fines Content in the Filter 52
4.5.4. Discussion on Numerical Results of Static Tests 54

CHAPTER 5. PARAMETRIC STUDY ON NUMERICAL MODEL 57
5.1. Introduction 57
5.2. Effect of Porosity of the Base Material on Filter Performance 57
5.3. Effect of Porosity of the Filter Material on Filter Performance 59
5.4. Effect of Permeability of the Filter Material on Filter Performance 60
5.5. Discussion on Parametric Study on Numerical Model 62

CHAPTER 6. CONCLUSION 64
6.1. Summary and Main Findings 64
6.2. Recommendations for Future Research 66

REFERENCES 68

LIST OF FIGURES

Figure **Page**

Figure 1.1 Different zoning in embankment dams (Source: Foster, 2000) 1
Figure 1.2 Atatürk Dam (Source: ataturkbaraji.com) 2
Figure 1.3 Cross-section of Kalabak Dam and possible cracks in the core of the dam 4
Figure 2.1 Mechanisms of internal erosion (Source: Robbins & Griffiths, 2018) 8
Figure 2.2 Process of failure caused by concentrated leak erosion (Source: Wan & Fell, 2004) 10
Figure 2.3 Teton Dam failure in 1976 (Source: 1976: Collapse of the Teton Dam in Idaho | History.info) 10
Figure 2.4 Erosion Boundaries (Source: Foster & Fell, 1999) 13
Figure 2.5 No Erosion Filter Test (Source: Sherard & Dunnigan, 1989) 14
Figure 3.1 Kalabak Dam before starting operation (Source: Aliağa Belediyesi (aliaga.bel.tr)) 16
Figure 3.2 NEF Test apparatus (Source: Ecemis, 2023) 18
Figure 3.3 Configuration of EPWPTs and SAs (Source: Ecemis, 2023) 18
Figure 3.4 Preformed 1mm diameter hole in the base samples (Source: Ecemis, 2023) 19
Figure 3.5 Filter and base samples of Kalabak Dam (Source: Ecemis, 2023) 20
Figure 3.6 Particle size distribution for the filter samples and the base sample 21
Figure 3.7 Change in (a) outflow rate, (b) inlet pressure, (c) outlet pressure, for the filter with FC of 0% 23
Figure 3.8 Change of water quality for the filter with FC of 0% (Source: Ecemis, 2023) 24
Figure 3.9 Final hole diameter (2 – 3 mm) for the filter with FC of 0% (Source: Ecemis, 2023) 24
Figure 3.10 Change in (a) outflow rate, (b) inlet pressure, (c) outlet pressure, for the filter with FC of 2% (Source: Ecemis, 2023) 25
Figure 3.11 Change of water quality for the filter with FC of 2% (Source: Ecemis, 2023) 26
Figure 3.12 Final hole diameter (1 mm) for the filter with FC of 2% (Source: Ecemis, 2023) 26

Figure **Page**

Figure 3.13 Change in (a) outflow rate, (b) inlet pressure, (c) outlet pressure, for the filter with FC of 5% 27
Figure 3.14 Change of water quality for the filter with FC of 5% (Source: Ecemis, 2023) 28
Figure 3.15 Final hole diameter (1 mm) for the filter with FC of 5% (Source: Ecemis, 2023) 28
Figure 3.16 NEF Test attached to shaking table (Source: Ecemis, 2023) 29
Figure 3.17 Input acceleration during sinusoidal excitations for frequencies of (a) 2Hz, and (b) 4Hz 29
Figure 3.18 Change in (a) rate of flow, (b) inlet pressure, (c) outlet pressure, and (d) measured acceleration for 2Hz frequency dynamic test 30
Figure 3.19 Change of water quality for 2Hz frequency dynamic test (Source: Ecemis, 2023) 32
Figure 3.20 Final hole diameter for 2Hz frequency dynamic test (Source: Ecemis, 2023) 32
Figure 3.21 Change in (a) rate of flow, (b) inlet pressure, (c) outlet pressure, and (d) measured acceleration for 4Hz frequency dynamic test 33
Figure 3.22 Change of water quality for 4Hz frequency dynamic test (Source: Ecemis, 2023) 34
Figure 3.23 Final hole diameter for 4Hz frequency dynamic test (Source: Ecemis, 2023) 35
Figure 3.24 Variation in Q of (a) static tests, (b) dynamic tests 37
Figure 4.1 CFD analysis of NEF Tests performed by Frishfields et al. (2011) (a) initial phase, and (b) transportation of base particles into pores of the filter (Source: Frishfields et al., 2011) 39
Figure 4.2 Configuration of NEF test used in the numerical models 41
Figure 4.3 3D view of the NEF model geometry 42
Figure 4.4 Created hole model in the base sample 42
Figure 4.5 Concentrated leak erosion mechanism (Source: Fell et al., 2014) 46
Figure 4.6 Outflow results of NEF tests conducted on (a) Horsetooth and (b) Many Farms Dams samples (Source: Dam Safety Office, 2004) 48

Figure **Page**

Figure 4.7 Numerical results of (a) Pore pressure distribution, (b) specific discharge and (c) hole displacement vectors, of the static test without fine particles in the filter 49
Figure 4.8 Comparison of outflow rates, Q of experimental (blue) and numerical (red) results for ST-1 50
Figure 4.9 Numerical results of (a) Pore pressure distribution, (b) specific discharge vectors, (c) hole displacement vectors, of the static test with 2% fines content in the filter 51
Figure 4.10 Comparison of outflow rates, Q of experimental (blue) and numerical (red) results for ST-2 52
Figure 4.11 Numerical results of (a) Pore pressure distribution, (b) specific discharge vectors, (c) hole displacement vectors, of the static test with 5% fines content in the filter 53
Figure 4.12 Comparison of outflow rates, Q of experimental (blue) and numerical (red) results for ST-3 54
Figure 4.13 Numerical results of change in (a) outflow rate, and (b) displacement of the hole in the static tests over time 56
Figure 5.1 The effect of porosity of the base on change in (a) outflow rate, and (b) displacement of the hole, over time 58
Figure 5.2 The effect of porosity of the filter on change in (a) outflow rate, (b) displacement of the hole, over time 60
Figure 5.3 The effect of permeability of the filter on change in (a) outflow rate, and (b) displacement of the hole over time 62

LIST OF TABLES

Table **Page**

Table 2.1 Filter design criteria (Source: Vakili et al., 2018) 11
Table 3.1 Base sample physical properties 20
Table 3.2 Filter sample physical properties 21
Table 3.3 Filter sample compaction and permeability values 21
Table 3.4 Water quality scale and abbreviations 22
Table 3.5 Summary of NEF tests 36
Table 3.6 Compliance of samples to the criteria 36
Table 4.1 Correlations for hydraulic conductivity 44
Table 4.2 Fluid model properties for materials 45
Table 4.3 Mohr-Coulomb material properties used in numerical analyses 46
Table 4.4 Test names performed in the lab 48
Table 5.1 Porosity, Biot modulus, and Biot coefficient used for the base material 57
Table 5.2 Porosity, Biot modulus, and Biot coefficient used for the filter materials 59
Table 5.3 Permeability values of filters and their performances 61

LIST OF SYMBOLS AND ABBREVIATIONS

$(\gamma_d)_{max}$	: Maximum dry unit weight
α	: Biot coefficient
a_{max}	: Maximum acceleration
c	: Cohesion
d_{15B}	: The particle size diameter where 15% by weight of base material is smaller
D_{15F}	: The particle size diameter where 15% of filter material is smaller
d_{85B}	: The particle size diameter where 85% of base material is smaller
d_{95B}	: The particle size diameter where 95% of base material is smaller
D_r	: Relative density
E	: Elasticity modulus
e	: Void ratio
ϕ	: Internal friction angle
FC	: Fines content
g	: Gravitational acceleration
G_s	: Specific gravity
i	: Hydraulic gradient
γ_s	: Saturated unit weight
γ_w	: Unit weight of water
k	: permeability
K	: Bulk modulus
K_w	: Bulk modulus of water
LL	: Liquid limit
M	: Biot Modulus
n	: Porosity
ν	: Poisson's ratio
NEF Test	: No Erosion Filter Test
PI	: Plasticity index
PL	: Plastic limit
Q	: Flow rate
q	: Specific discharge
ρ_w	: Density of water
S	: Saturation degree
w	: Water content
w_{opt}	: Optimum water content

CHAPTER 1

INTRODUCTION

1.1. General

Dams are one of the most common structures in human history. They are mainly built to store water for irrigation, hydroelectric power generation, and flood control. It is one of the most fundamental parts of human civilization, so there are thousands of dams around the world. Because of the uniqueness of the site, design engineers should choose the appropriate dam type based on the geography, climate, available materials, accessibility, river currents, and seismic activities at the site where the dam is planned to be built.

There are four types of dams: arch dam, buttress dam, embankment dam, and gravity dam. Arch dams are made of concrete, while gravity dams and buttress dams are made from masonry or concrete. On the other hand, in the embankment dams, natural materials are used. Various types of embankment dams have been developed using different zoning shown in Figure 1.1. The decision should be made by considering the site conditions and the materials that can be used in the vicinity of the site.

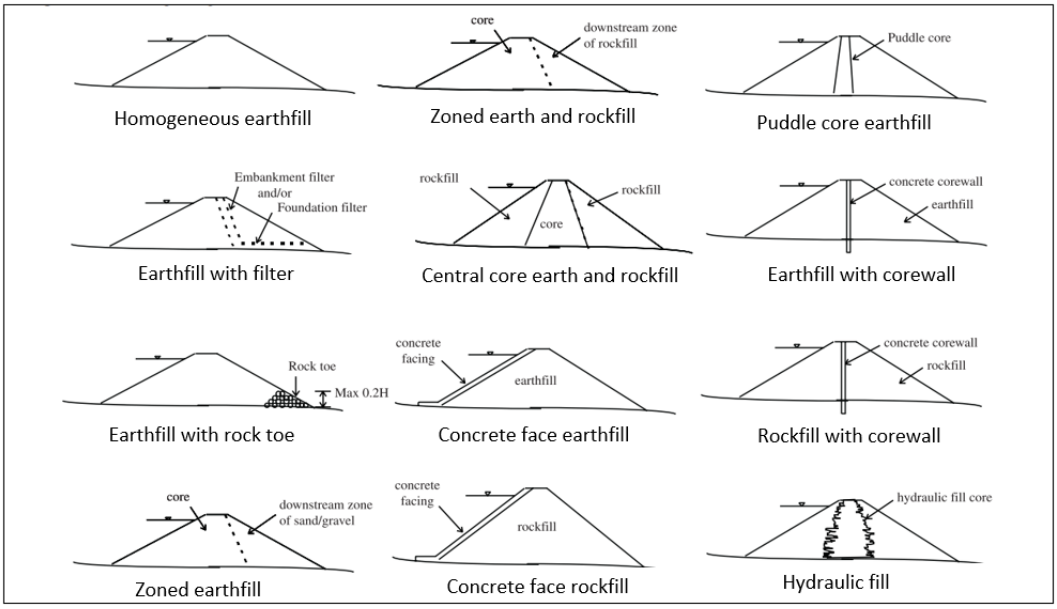

Figure 1.1 Different zoning in embankment dams (Source: Foster, 2000)

Embankment dams have plenty of advantages of being built on any foundation that other types of dams cannot adapt to and using natural materials that get cheaper than dams made of concrete. Usually, the compositions of clay, silt, sand, gravel, and rock boulders are used in this type of dam, and these materials can be excavated on the site or found in nearby quarries, speeding up the construction process. Thanks to these advantages, numerous embankment dams exist worldwide. According to the information taken from CİMER (Presidency of the Republic of Türkiye Directorate of Communications), 1505 embankment dams have been completed in Türkiye, and the biggest one is Atatürk Dam which is shown in Figure 1.2.

Figure 1.2 Atatürk Dam (Source: ataturkbaraji.com)

Despite the advantages of embankment dams, there are critical disadvantages related to their safety. Except for human activities, natural events may affect embankment dams negatively. Zhang et al. (2009) studied different types of dams that failed, and the reasons for failure can be summarized as:

- Flood and prolonged periods of precipitation (i.e. Archusa Creek Dam failure in 1998, (Newhouse, 2010)),
- Imperfection due to poor compaction,
- Differential settlement of the dam,
- Over-topping,

- Internal erosion (piping),
- Inadequate management, and
- Earthquake

It has been revealed from statistical studies that piping is the most common one in the failure of dams (Foster, 2000). It can occur in different parts of dams, and varied factors can trigger internal erosion. For this reason, understanding the behavior of soil and water covering all the factors, including hydrodynamic forces and effective stress together, is crucial for dam safety.

Filters or drains are a practical way to control seepage through the dam. If appropriately designed, they can prevent internal erosion with retention and permeability functions which were described in the next chapter (ICOLD, 2017). Their usage is common in embankment dams. However, failure due to piping occurred even if there were filters in the dam (Foster, 2000).

Many researchers studied the design of filters with the help of laboratory tests to understand the interaction between core material, filter material, and water. One of the most valuable tests is the No Erosion Filter Test (NEF Test), which was developed by Sherard et al. in 1989. NEF Test is accepted in the literature as the most proper method to determine the critical filter that leans on the impermeable core material in the downstream side of an embankment dam. In the NEF test, the most severe condition is represented as an erosive leak from the core material to the filter material (Shourijeh, 2018).

1.2. Motivation of the Thesis

The behavior of soils and water flow through the soils are complex issues in the geotechnical engineering practice. The interface between materials in the embankment dams is also complex due to having different pores, permeability values, high hydraulic gradients, and variations in pore pressures. Additionally, pore pressure variation resulted in deformations. (Ma et al., 2022). It is essential to figure out this complex interaction of water and soil together. There are different experimental studies to understand the interaction developed for different internal erosion mechanisms: suffusion, concentrated leak erosion, backward erosion, and contact erosion defined in CHAPTER 2. To lessen laboratory effort and save time by conducting several sets of experiments, many

researchers modeled the internal erosion for different mechanisms by using the finite element method (FEM), finite difference method (FDM), computational fluid dynamics (CFD), discrete element method (DEM), smoothed-particle hydrodynamics (SPH) and analytical approaches. However, there is still a need for research on the numerical modeling of internal erosion. In the literature, the concentrated leak erosion mechanism and its detection through the NEF test have not been investigated by using the finite difference method. It has been provided a simulation of the NEF test and how to evaluate filter sand performance based on numerical modeling in this study.

This thesis investigates the concentrated leak erosion mechanism by numerical modeling of a series of NEF tests performed in the Izmir Institute of Technology geotechnical laboratory. It is aimed to understand the internal erosion of base material and the effect of fines content of filter material on internal erosion resistance. The materials used in the NEF tests belonged to Kalabak Dam, whose cross-section and a possible crack that may form due to hydraulic fracturing and differential settlement and lead to initiate concentrated leak erosion mechanism shown in Figure 1.3. The physical properties of the base and the filter materials, which are detailed in the related sections, were obtained from the TUBITAK Project No. 221M071 (Ecemis and Valizadeh, 2023). Numerical simulations of the tests were modeled by using the commercially available software FLAC3D which uses the finite difference method (Itasca Consulting Group, Inc., 2017).

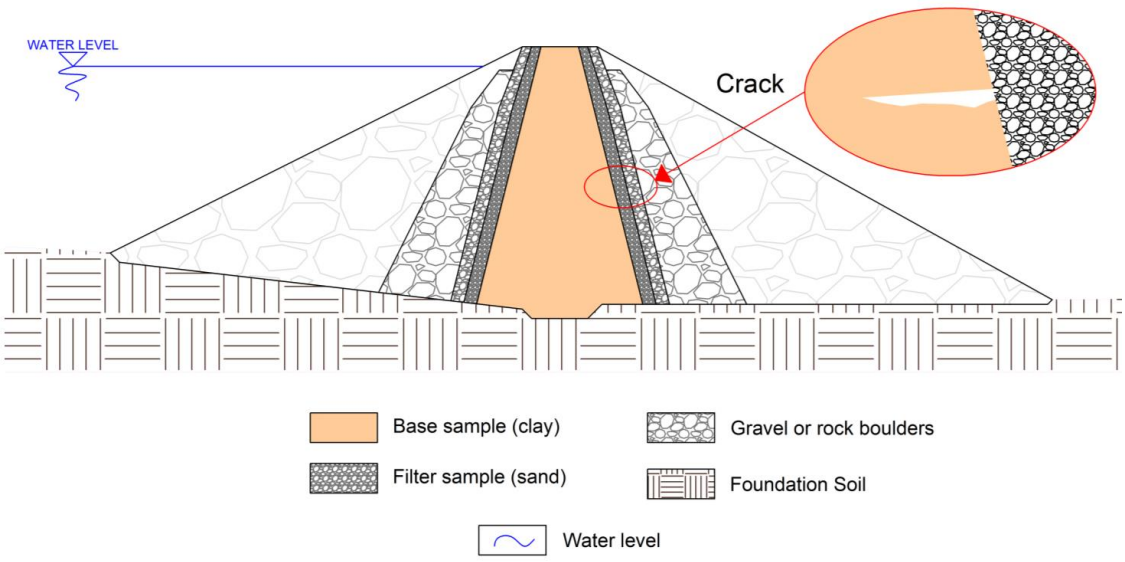

Figure 1.3 Cross-section of Kalabak Dam and possible cracks in the core of the dam

1.3. Organization of the Thesis

In the scope of this thesis, numerical modeling of the NEF test in FLAC3D and evaluation of filter sand performance through the models are aimed.

This thesis consists of six chapters in total:

(1) The first chapter introduces the importance and types of dams and the pros and cons of embankment dams. Additionally, the objective of the study is mentioned.

(2) The second chapter presents a literature review of internal erosion, filter design, and NEF tests in detail. Mechanisms and process of internal erosion, prevention of it by filtering embankment dams, selection of appropriate filter, and the application and evaluation of NEF test are explained.

(3) The third chapter presents NEF tests performed in the scope of the TUBITAK Project (No. 221M071). The materials, setup of the apparatus, results, and assessment of the tests are given.

(4) The fourth chapter involves the concept of numerical modeling of NEF test in FLAC3D. Geometry, material models, boundary conditions, and outcomes of the analyses are presented.

(5) The fifth chapter consists of conducted parametric studies. First, the porosity of the filter and the base materials, and the permeability of the filter are investigated. Then, numerical results are compared with each other. Filter sand performance is decided as successful or unsuccessful based on the results.

(6) The sixth chapter summarizes the internal erosion mechanism, the numerical modeling of the NEF test, and the results. Finally, the recommendations and main findings for future research are given.

CHAPTER 2

LITERATURE REVIEW OF INTERNAL EROSION

2.1. Introduction

This chapter examines the review of the internal erosion concept, filter design in embankment dams, and the NEF test. The safety issues of internal erosion and its mechanism and progression are detailed in the next section. After that, the dam filter's importance and functions are explained. Besides, the chronology of filter design criterias proposed by several researchers is given. In the following chapter, the NEF test method to evaluate filter sand performance is mentioned. Finally, the difference of this study from the other studies is concluded in the last section.

2.2. Internal Erosion Phenomena in Embankment Dams

It has been known from failure cases in history due to internal erosion that filtering of the dam is vital. The statistical investigation of 11192 embankment dams revealed that more than 50% of dam failures had been caused by piping (Foster et al., 2000 and Zhang et al., 2016).

It can happen in various locations of the dam, as listed below (FEMA, 2011).

- Thorough dam body (embankment),
- Along the interface between embankment and abutment,
- Along the interface between the embankment and foundation,
- Cutoff trenches

Technically and economically, it is hard to detect internal erosion and piping due to occurring under the surface. After the roof settles, it can be evitable on the surface (Bernatek-Jakiel & Poesen, 2018). The process starts slowly, and if it cannot be stopped by filtering, it gets faster with the increase in speed of the particle loss in the core. Eventually, with breaching, the progress of internal erosion reaches the point of no return and causes sudden failure of the dam (Hellström, 2009). This process is divided into four stages: initiation, continuation, piping formation, and breaching.

Internal erosion initiates caused by different mechanisms based on soil type and particle size distribution, compaction effort, nature of foundation soil, heavy rainfall, floods, and the like. The four main mechanisms defined in the literature are suffusion, backward erosion, concentrated leak, and contact erosion. The initiation mechanisms are summarized below and represented in Figure 2.1.

- **Suffusion:**

  It is the mechanism that transportation of fine particles throughout the soil via water flow to the pores of coarser materials. When the flow velocity applies adequate stress to the soil, it causes an increase in the effective stress of coarser particles. If the bearing capacity cannot stand these high stresses, collapse occurs (Scheperboes et al., 2022).

- **Backward erosion:**

  It is the mechanism that happens at the toe of the dam. High hydraulic gradients at the exit downstream cause movement of the particles toward the reservoir. In cohesive foundation soils, the roof forms, and like a channel, water continues to flow under the dam (Bonelli, 2013).

- **Concentrated leak erosion:**

  It is the mechanism that can initiate internal erosion due to transverse cracks. The relatively high water velocity enhances the hydraulic gradient at these cracks, and it causes the progressive movement of particles (Caldeira, 2018). The cracks generally provoke by differential settlement and hydraulic fracturing.

- **Contact erosion:**

  It is the mechanism that occurs in the contact where the interface between coarser and finer materials is. Fine particles are eroded by lateral flow into the coarser material and cause segregation (Bonelli, 2013, and Fry 2016). It initiates when two conditions, geometrically and hydraulically which are the largeness of pores in coarser material than finer material and adequate flow velocity to erode finer grains (Robbins, 2018), are encountered.

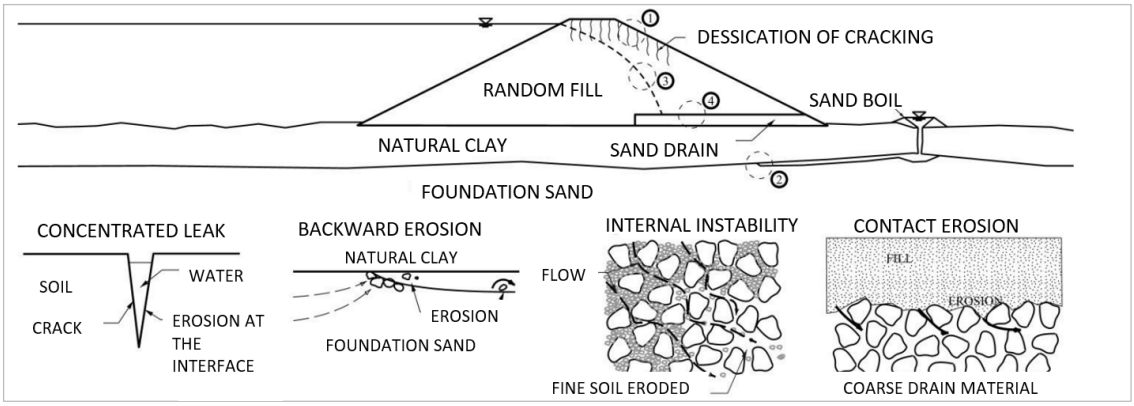

Figure 2.1 Mechanisms of internal erosion (Source: Robbins & Griffiths, 2018)

Soil characteristics influence resistance to internal erosion, and Stephanie classified susceptibility of soil nature in 2013 as plastic soils, dispersive soils, and non-plastic soils. In plastic soils which consist of clay, contact erosion, and concentrated leak erosion mechanism tend to occur. The cracks are saved by clay, but the clay particles are eroded through the crack when the flow velocity is enough to carry. Due to the chemical properties of clay and soil in dispersive soils, also plastic, internal erosion can be inducted in a concentrated leak mechanism even with low gradients and stresses. Non-plastic soils such as gravel, sand, and silt cannot hold the cracks and collapse. These particles are erodible with backward erosion, contact erosion, and suffusion mechanisms. As the weight of the particle increases, it becomes harder to erode the particle. Particle size distribution also influences erosion resistance.

Delgado-Ramos et al. (2012) scrutinized plasticity, clay mineralogy, the water content of base soil, hydraulic gradient, and additives' influence on internal erosion. Whereas high water content and hydraulic gradient caused erodible behavior for base materials, plasticity showed no effect on erosion resistance.

The continuation of internal erosion follows its initiation. In this phase, filtering and zoning in the dam should play their role. Based on this, erosion may be stopped (no-erosion), may be stopped after a slight movement of particles (some erosion), may be stopped after a large particle movement (excessive movement), and may not be stopped (continuing erosion) (Foster & Fell, 1999). The filter behavior is described in detail in the next section.

In the case of continuing erosion, the progression phase comes at which pipe is formed in each mechanism except suffusion. It is the phase at which internal erosion can be detected easily in the dam by checking variations in pore water pressure and stress

(Wang et al., 2016). In contact erosion, finer material particles fill in the pores of coarser material, and a pipe may improve in the finer material. In concentrated leak erosion, erosion through the crack or flaw creates a pipe. In backward erosion, the particles follow a path to the upstream side of the dam beneath the soil; if it reaches the reservoir, a pipe develops. On the other hand, pipe formation is not observed in suffusion, and soil permeability may rise considerably. Before breaching, if the pipe or flow path is observed, the detection of location and successful prevention in time are of high concern (Fell, 2003).

In the last phase of internal erosion, breaching occurs with a widening of the pipe. Evidence like settlements in the crest, a landslide of the downstream surface, sand boils at the downstream point where backward erosion has initiated, and the like can be clearly observed. Consequently, with the high-volume loss of materials, the dam reservoir fails. The resulting damage may be catastrophic depending on the volume of water stored in the reservoir. For large dams and reservoirs, failure can often cause severe damage and even loss of life (Graham & Wayne, 1999).

2.3. Filter Design Criteria

It has been stated that internal erosion is triggered when the base particles are transported with fluid flow to the filter material; if it continues, it may cause dam failure. In the scope of this study, the concentrated leak mechanism has been scrutinized, and the proper filter design to prevent it is detailed. The general process leading to dam failure due to concentrated leak erosion is demonstrated in Figure 2.2. An example of the enormous weight failure can be seen in Figure 2.3, which is the failure of Teton Dam caused by internal erosion developed by a concentrated leak mechanism. Therefore, it is clear that the downstream filter in the dam plays a critical role in safety. Many researchers have attempted to understand the relationship with core material to design effective filters.

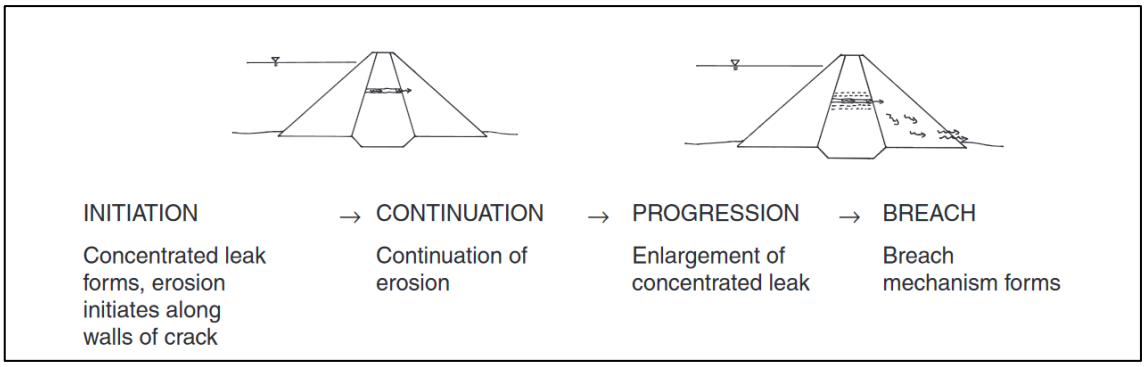

Figure 2.2 Process of failure caused by concentrated leak erosion (Source: Wan & Fell, 2004)

The general concept of the filter is being non-cohesive, with proper coarseness and fineness, because non-cohesive materials cannot maintain any crack so that the filter material can close the cracks inside of it; coarse materials have higher permeability, so the filter lets seepage flow through itself, and fineness provides self-filtration to filter (Indraratna et al., 2004).

Figure 2.3 Teton Dam failure in 1976 (Source: 1976: Collapse of the Teton Dam in Idaho | History.info)

The first criteria recommended by Terzaghi (1922) has led up filter design research in the literature. Two functions of the filter were considered, and the gradation of the base and filter should satisfy the relationships (Fannin, 2008) given below:

i) The sealing function of the filter to prevent the transition of base particles to the pores of the filter:

$$\frac{D_{15F}}{d_{85B}} \leq 4 \quad (2.1)$$

ii) Seepage control through the dam function of filter to prevent excess pore water pressure:

$$\frac{D_{15F}}{d_{85B}} \geq 4 \quad (2.2)$$

However, the criteria given by Terzaghi have been proposed for non-cohesive uniform base soils, so using it in other soils is inappropriate.

After Terzaghi, other researchers developed their criteria from their laboratory and theoretical studies. Properties such as permeability, fines content, plasticity, dispersity, and particle size have been considered, and plenty of criteria have been proposed as a result of their precious effort (Vakili et al., 2018). Thus, safer design of dams has been studied, and several criterias were proposed. All of the proposed filter design criteria are summarized in Table 2.1.

Among all of these criterias given in Table 2.1, the criteria Sherard and Dunnigan proposed in 1989 is notable because the laboratory study and the enhanced experiments are still helpful and provide a practical filter design.

Table 2.1 Filter design criteria (Source: Vakili et al., 2018)

Criteria proposed by	**Base soil**	**Criteria**	
		For non-dispersive base soils	**For high-dispersive base soils**
Terzaghi (1926)	Non-cohesive uniform	$D_{15f} \leq 4.0–5.0\ d_{85}$	Not valid
Bertram (1940)	Silt and fine sand	$D_{15f} \leq 6.0\ d_{85}$	Not valid
Vaughan and Soares (1982)	Clay	$k_f = 6.7 \times 10^{-6} \times (d_R)^{1.52}$	Not valid
Sherard and Dunnigan (1989)	FC ≥ 85% FC = 40 - 85% FC < 15% FC = 15 - 40 %	$D_{15f} \leq 9\ d_{85}$ $D_{15f} \leq 0.7$ mm $D_{15} \leq 4d_{85}$ $D_{15} \leq \frac{40-FC}{25}(4d_{85} - 0.7) + 0.7$	
Khor and Woo (1989)	FC = 40 - 85%	$D_{15F} \leq 12\ d^{*}_{85}$	Not valid
Lafleur et al. (1993)	Cohesive	$D_{15F} \leq 0.4$ mm	$D_{15F} \leq 0.2$ mm
Foster and Fell (2001)	FC ≥ 85 % FC = 35 - 85%	$D_{15F} \leq 9\ d_{85}$ $D_{15F} \leq 0.7$ mm	$D_{15F} \leq 6.5\ d_{85}$ $D_{15F} \leq 0.5$ mm
Locke and Indraratna (2002)	FC ≥ 85% FC = 40 - 85%, PI > 10 FC = 40 - 85%, PI < 10	$D_{15F} \leq 12\ d_{85reduced}$ $D_{15F} \leq 9\ d_{85reduced}$ $D_{15F} \leq 4\ d_{85reduced}$	Not valid Not valid Not valid

(cont. on next page)

Table 2.1 (cont.)

Criteria proposed by	Base soil	Criteria	
		For non-dispersive base soils	For high-dispersive base soils
Locke and Indraratna (2002)	FC ≥ 85%	$D_{15F} \leq 12\ d_{85reduced}$	Not valid
	FC = 40 - 85%, PI > 10	$D_{15F} \leq 9\ d_{85reduced}$	Not valid
	FC = 40 - 85%, PI < 10	$D_{15F} \leq 4\ d_{85reduced}$	Not valid
Fell et al. (2005)	FC ≥ 85 %	$D_{15F} \leq 9\ d_{85}$	$D_{15F} \leq 6\ d_{85}$
	FC = 35 - 85%	$D_{15F} \leq 0.7$ mm	$D_{15F} \leq 0.5$ mm
Delgado-Ramos et al. (2006)	FC ≥ 40%	$k_f = 59.728 \times e^{(-0.102 \times FC)}$	Not valid
Shourijeh and Soroush (2009)	FC ≥ 85 %	$D_{15F} \leq 9\ d_{85}$	$D_{15F} \leq 7.5\ d_{85}$
	FC = 80 - 85%	$D_{15F} \leq$ min(0.7 mm, $6.4 \times d_{85}$)	$D_{15F} \leq 0.5$ mm
	FC = 35 - 80%	$D_{15F} \leq 0.7$ mm	$D_{15F} \leq 0.5$ mm
Vakili et al. (2015)	FC = 40 - 85%, D<20%	$D_{15f} \leq 0.6$ mm	$D_{15F} \leq 0.6$ mm
	FC = 40 - 85%, %20≤D≤ 65%	$D_{15F} \leq 0.5$ mm	$D_{15F} \leq 0.5$ mm
	FC = 40 - 85%, D≥65%	$D_{15F} \leq 0.28$ mm	$D_{15F} \leq 0.28$ mm
Vakili et al. (2015)	FC ≥ 85 %	$D_{c35}/d^*_{85} \leq 1.25$	$D_{c35}/d^*_{85} \leq 1.25$
	FC = 40 - 85%	$D_{c35}/d^*_{85} \leq 1.0$	$D_{c35}/d^*_{85} \leq 0.5$

Note: D: dispersity, d^*_{85}: modified particle size distribution curve, D_{c35}: constriction size (limit)

Basically, Foster and Fell (1999) defined the success of the filter in three categories: (1) no erosion in which no erosion happens; (2) some erosion, where the filter prevents erosion after "some" erosion and (3) continuing erosion, which is the riskiest, in which the filter cannot stop the erosion, and it continues until failure. Additionally, they have shown these boundaries depending on $D_{15F,}$ represented in Figure 2.4.

The erosion boundaries can be identified through the NEF test and Continuing Erosion test (CEF test). CEF test is another test method to identify internal erosion. The difference between the two tests is the usage of coarser filters, thicker base specimens, and collection of eroded base materials to define how much material cause the filter sealing (Foster & Fell, 1999).

No erosion boundary is the limit that while a smaller D_{15F} will show no visible erosion, a larger D_{15F} will erode. It is defined through the NEF tests in different combinations of base-filter samples until finding the "D_{15Fb}" value, which is defined based on fines content of the base and D_{15F} and D_{85B} of the combinations. (Tham, 2020 and Foster&Fell, 2001).

Foster and Fell (2001) defined excessive and continuing boundaries by proposing criterias based on d_{95B} value of the base soil by conducting CEF tests. Based on the CEF

test results, D_{15F} and %fine-medium sand of the base soil is plotted, then D_{15F} that causes erosion losses between 0.1 g/cm^2 to 1.0 g/cm^2 is obtained (Tham, 2020).

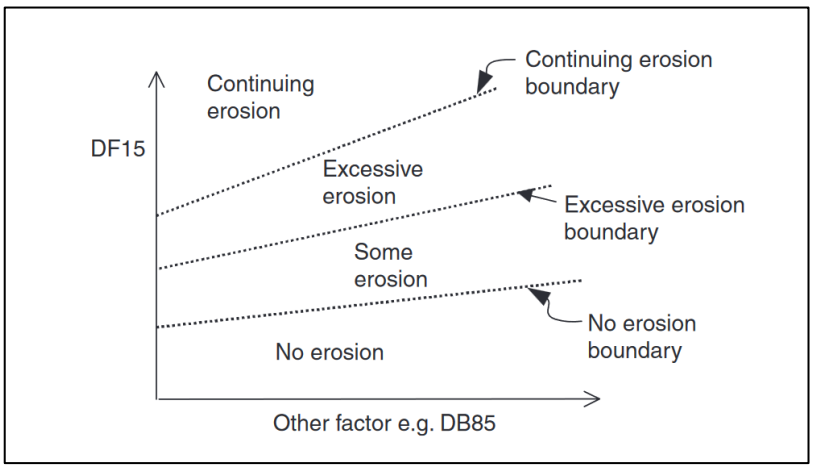

Figure 2.4 Erosion Boundaries (Source: Foster & Fell, 1999)

It has been pointed two issues required to be answered for dam safety by Foster and Fell (1999):

i) Can the filter prevent erosion if the leakage begins through the base?

ii) If the filter seals that leakage, how much time can the dam handle it, and how much base material will erode until sealing?

The success of the filter depends on its ability to eliminate internal erosion. To reach that functionality, it must be stable, maintain its gradation and not react chemically, biologically, or physically (ICOLD, 1994). Therefore, its design and construction stages running properly have great importance for dam safety.

2.4. No Erosion Filter (NEF) Test

The accepted method in the literature to detect concentrated leakage was developed by Sherard and Dunnigan (1984). In their study, they conducted a series of slot and slurry tests with different mechanisms but the same goal and gave similar results in evaluating filter sand performance. The outcome of their study has demonstrated that based on the erosion mechanism, the downstream filter has been decided as critical, so clogging of cracks and controlling the seepage through the base are the functions of that filter. Then, the influence of particle size distribution, dispersity, and Atterberg limits on internal erosion resistance was investigated.

Sherard and Dunnigan evaluated filter sand performance based on outflow rate, clearwater observation, and the diameter of the preformed hole. It has been seen that the flow rate coming from the outlet of the apparatus has declined and stabilized, and clearwater observation followed it in successful filters. On the other hand, clearwater has not been observed in unsuccessful filters, and a high flow rate continued during the whole test. The filter has been judged in the first 2 to 3 minutes. Another apparent evidence of erosion and unsuccessful filters is the increase in hole diameter. The eroded particles in the base sample are transported with the water flow, resulting in constant dirty water.

After the investigation of sand performance through the slot and the slurry tests, Sherard and Dunnigan (1989) worked up No Erosion Filter (NEF) Test series to see the behavior of coarser base soils (d_{85B} >> 0.1 mm). The essential part of this test is the 1 mm diameter hole which was created to represent the possible cracks in the base sample before the test. Therefore, it is easy to see the particle loss from the hole's walls with enlargement in the diameter. The schematic view of the test setup given by Sherard and Dunnigan (1989) is represented in Figure 2.5. After high pressurized water application from the inlet of the apparatus, approximately 400 kPa, outflow rate, and clearwater were observed.

In the series of the NEF tests Sherard and Dunnigan conducted, four groups of base soil have been identified depending on their particle size distribution. The internal erosion resistance of different soils has been examined, and it is decided that NEF Test provides the harshest state for the vulnerability of base particles of the dam to erosion.

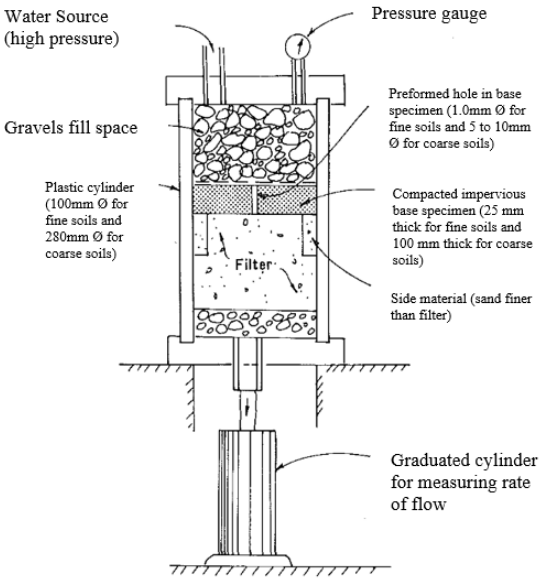

Figure 2.5 No Erosion Filter Test (Source: Sherard & Dunnigan, 1989)

In the continuation phase of internal erosion, four possibilities are mentioned based on filter performance: no erosion, some erosion, excessive movement, and continuing erosion. To commentate on it, the classification of contributed outflow, change in hole diameter, and the pressure change in the inlet where pressurized water is applied is recorded and observed. Three criterias were defined in order to accept the filter as "successful" by Soroush and Shourijeh (2009):

(1) Stabilizing or decreasing the trend of the rate of exit water flow

(2) Clearwater observation at the end of the test

(3) Barely any change in the preformed hole diameter

Progressive clearance of water can be qualified as very dark (VD), dark (D), moderately dark (MD), slightly dark (SD), barely visible (BV), clear (V), and perfectly clear (PC) (Raeisosadat et al. 2022). Examples of this rating system are given in the next chapter, which details the NEF test results conducted in the geotechnical laboratory of İzmir Institute of Technology.

2.5. Conclusion

In the previous chapters, the concept of internal erosion and filter design in embankment dams to mitigate internal erosion risk, and the NEF test method to evaluate filter sand performance are explained. To contribute the research of internal erosion, the series of the NEF tests are modeled by using the finite difference method in FLAC3D. Different mechanisms of internal erosion have been modeled by researchers using other methods. However, finite difference modeling of concentrated leak erosion mechanism needs to be researched due to the lack of study in the literature. Therefore, it is aimed to evaluate filter sand performance through the NEF tests in numerical models.

CHAPTER 3

NO EROSION FILTER (NEF) TEST

3.1. Introduction

This chapter summarizes the soil data obtained from the experimental studies and the NEF tests conducted in the scope of the TUBITAK Project (No. 221M071, Ecemis and Valizadeh 2023). Hence the experiments given in this chapter were performed by Valizadeh. Materials used in the NEF tests, test apparatus, and experiment process and results are given in detail. Finally, the NEF test results are presented and compared to each other.

The filter and the base samples belonging to Kalabak Dam (Figure 3.1) and the filter samples of Rahmanlar Dam in İzmir, Türkiye, were brought to the geotechnical laboratory of İzmir Institute of Technology, and their physical properties were identified. Then, the experimental setup was completed, and NEF tests were performed by following studies in the literature.

Figure 3.1 Kalabak Dam before starting operation (Source: Aliağa Belediyesi (aliaga.bel.tr))

3.2. Test Setup

A total of three static NEF tests and two dynamic NEF tests were performed. Whereas the effect of fines content (FC) was investigated in static tests, the effect of acceleration frequency (f) during cyclic loading was the variable in dynamic tests. Filter samples were mixed with different amounts of fines (silt) in static tests, and the best performance was obtained for 5% silt content based on the results for the materials belonging to Kalabak Dam and Rahmanlar Dam. Therefore, filter materials contained 5% silt content in dynamic tests, and they were tested for 2Hz and 4Hz frequencies. Finally, the Sherard & Dunnigan criteria (1989) compliance and the filter material's success were compared.

To define the physical properties of the filter and base materials of Kalabak Dam, sieve analysis, constant head test, and Standard Proctor test were performed on the collected samples. Finally, the apparatus was set up, and the samples of the materials were placed to perform the NEF tests.

3.2.1. NEF Test Apparatus

The apparatus components are shown in Figure 3.2. The inlet part of the apparatus has a water valve, pressure gauge, and inlet disk. The pressurized water comes from the valve, the gauge measures the pore pressure, and the disk is used to immobilize the samples, not to form cracks, deformation, and bending. The plexiglass cell is where the filter, base, and gravel samples are placed, and the pressurized water goes through. The diameter of the cell is 10 cm, and the length is 35 cm. During the test, the restraining rods and apparatus legs prevent the moving of the apparatus and the plexiglass cell. The last part is the outlet, where the water seepage is observed. An outlet disk is used for the same purpose as the inlet disk.

In addition to the main parts of the apparatus, two excess pore water pressure transducers (EPWPT) and two submersible accelerometers (SA) are utilized inside the samples to measure excess pore water pressure and acceleration during the test. They are connected to the data acquisition box (DAQ) to collect data. SAs are used in the dynamic tests. The configuration of instruments with test apparatus is demonstrated in Figure 3.3

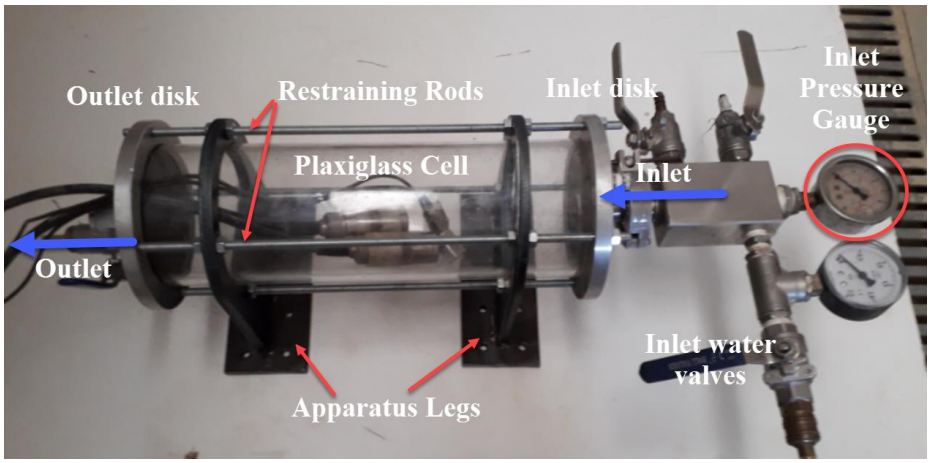

Figure 3.2 NEF Test apparatus (Source: Ecemis, 2023)

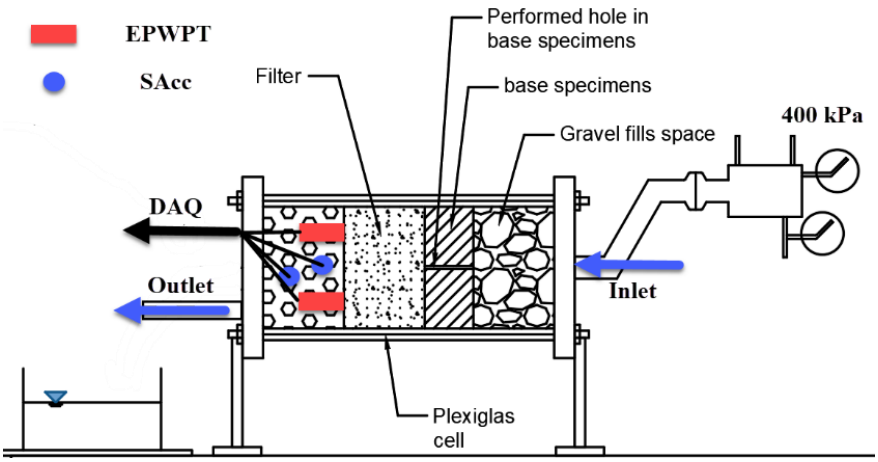

Figure 3.3 Configuration of EPWPTs and SAs (Source: Ecemis, 2023)

According to the study conducted by Sherard and Dunnigan (1989), it has been stated that the base soil thickness depends on whether it is coarse or fine and the diameter of the plexiglass cell. In this case, because of having fine particles in the base samples and the satisfaction ¼ aspect ratio of base thickness to the diameter, the thickness of the base was chosen as 25 mm.

A hole was created through the base sample for all tests to simulate the critical condition in the dam, which is the crack in the base sample on the downstream filter side. As shown in Figure 3.4, the diameter of the hole has been proposed as 1 mm in the finer base sample (Sherard & Dunnigan, 1989).

As aforementioned, the thickness of the base sample was chosen as 2.5 cm, as suggested for fine materials based on aspect ratio. In order to prevent internal erosion in the test, theoretical studies demonstrated that a few centimeters of thickness are appropriate (Witt, 1993). However, the thickness of the filter samples was chosen to be 10 cm.

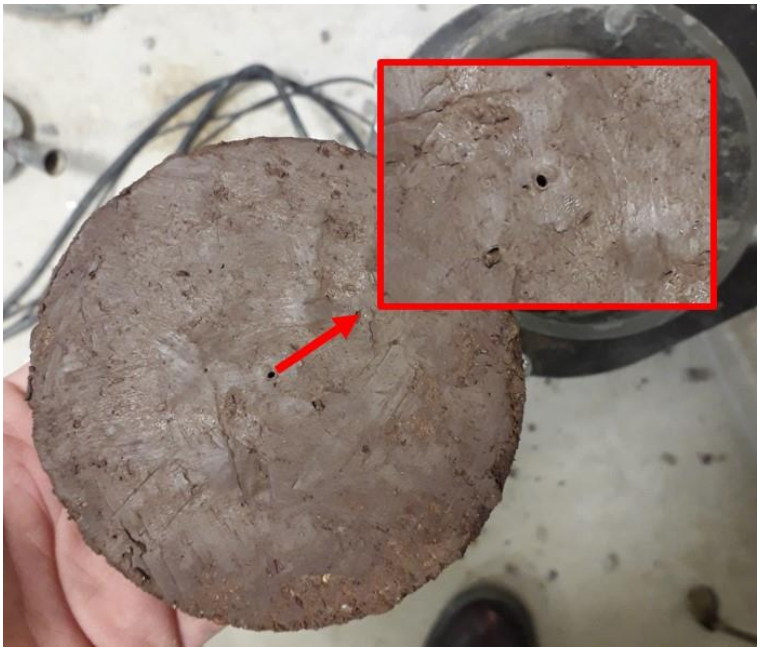

Figure 3.4 Preformed 1mm diameter hole in the base samples (Source: Ecemis, 2023)

3.2.2. Base and Filter Materials Used in the NEF Tests

The base and filter samples taken from Kalabak Dam in Aliağa, İzmir, Türkiye were brought to the geotechnical laboratory of IZTECH, and their physical properties were defined (Figure 3.5). Sieve analysis, hydrometer test, Atterberg limit tests, Standard Proctor test, hydraulic conductivity test, and specific gravity test were performed on the samples. The results and preparation of the samples are given for the base and the filter samples in the subtitles, respectively.

Figure 3.5 Filter and base samples of Kalabak Dam (Source: Ecemis, 2023)

3.2.2.1. Base Samples

Obtained $(\gamma_d)_{max}$, w_{opt}, G_s, LL, PL, and PI values are given in Table 3.1. Based on these laboratory experiments, the base material is classified as High Plastic Clay, CH, and D_{85} is found as 0.11 mm, which is used to check compliance with design criterias later. The base material was compacted in a container outside the apparatus and placed into the plexiglass cell.

Sherard and Dunnigan (1989) and Foster and Fell (2001) classified base soils as Group 1, 2, 3, and 4 which are given in Table 2.1. Based on this classification, Kalabak Dam base material belongs to Soil Group Number 2 because approximately 81% of the sample consisting fines grains which have smaller particles than sieve No. 200. Particle size distribution of the base sample is given in Figure 3.6 together with the filter samples.

Table 3.1 Base sample physical properties

Gs	**Atterberg Limits**			**Compaction**		**D_{85}**
	LL (%)	**PL (%)**	**PI (%)**	**$(\gamma_d)_{max}$ (kN/m^3)**	**w_{opt} (%)**	**mm**
2.61	62	27	35	18.7	17.8	0.11

3.2.2.2. Filter Samples

The variable in the NEF test series was the fines content of the filter material. Therefore, constant head tests were performed to obtain permeability in addition to sieve analysis and the Standard compaction test. The data and gradation curve for filter samples are presented in Table 3.2, Table 3.3, and Figure 3.6 below. The samples are classified as Clean Sand consisting of small amount of finer particles.

Table 3.2 Filter sample physical properties

FC	G_s	D_{10}	D_{15}	D_{30}	D_{60}	C_u	C_c	Classification
%	-	mm	mm	mm	mm	-	-	
0	2.56	0.23	0.36	0.71	1.75	7.6	3.8	Clean Sand - Poorly Graded (SW-SP)
2	2.56	0.18	0.32	0.67	1.75	9.7	4.4	Clean Sand (SW-SP)
5	2.56	0.17	0.31	0.66	1.75	10.3	4.5	Clean Sand (SW-SP)

Table 3.3 Filter sample compaction and permeability values

FC	$(\gamma_d)_{max}$	w_{opt} (%)	e_{max}	e_{min}	D_r	k
%	(kN/m^3)	%	-	-	%	(cm/sec)
0	19.0	13.0	0.520	0.320	80	0.00112
2	19.4	12.7	0.520	0.320	80	-
5	19.9	12.1	0.518	0.310	80	-

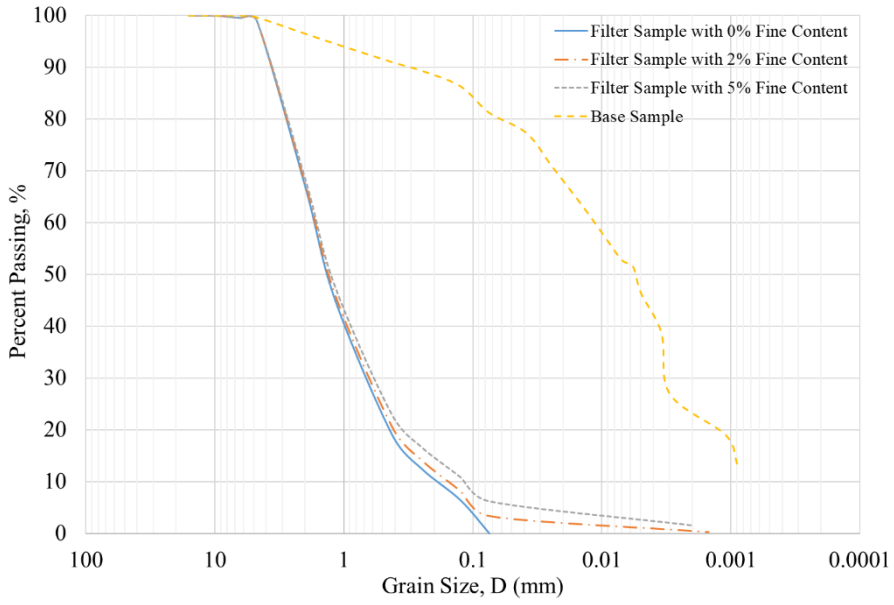

Figure 3.6 Particle size distribution for the filter samples and the base sample

3.3. Static Tests

Under static conditions, a total of three NEF tests were performed. The variable in the static series was the fines content of the filter sample. The first sample did not contain fine particles. The others include 2% and 5% FC, respectively. The results and observations are detailed for each test in the following sections. Additionally, water quality observations are noted in the graphs based on the scale given with abbreviations in Table 3.4. In addition to water quality, the time at which the clearwater is observed is marked as a green line on the outflow rate graphs (Figure 3.7a, Figure 3.10a, Figure 3.13a).

Table 3.4 Water quality scale and abbreviations

Water Quality						
Very Dark	Dark	Moderately Dark	Slightly Dark	Barely Visible	Clear	Perfectly Clear
VD	D	MD	SD	BV	C	PC

3.3.1. Static Test without Fine Particles (FC = 0%)

The first test of the static series was conducted on the filter material with no fine particles. The sample of clean sand with optimum water content was placed into the plexiglass cell by compacting it until having 80% relative density (D_r). When the preparation was completed, 400 kPa pore water pressure was applied from the inlet of the apparatus (schematically shown in Figure 4.2). At the beginning of the test, the flow rate was high, so the pressure in the inlet dropped sharply; the pressure in the outlet was measured at around 4.91 kPa during the test. Clearwater was observed at the end of 7 minutes with a flow rate of 418 ml/min, and the test was ended after 10 minutes. After the completion of the NEF test, it was seen that the hole diameter was increased from 1 mm to 3 mm (Figure 3.9), which is caused by the loss of particles in the base sample due to erosion. The change in flow rate, inlet, and outlet pressures are shown in Figure 3.7a-c. The change in water quality during the test and the measured diameter of the hole after the test can be observed in Figure 3.8 and Figure 3.9. Consequently, due to observing enlargement in the hole diameter, and an increasing trend in high flow rate, the clean filter sample has been evaluated as unsuccessful based on the evaluation criteria.

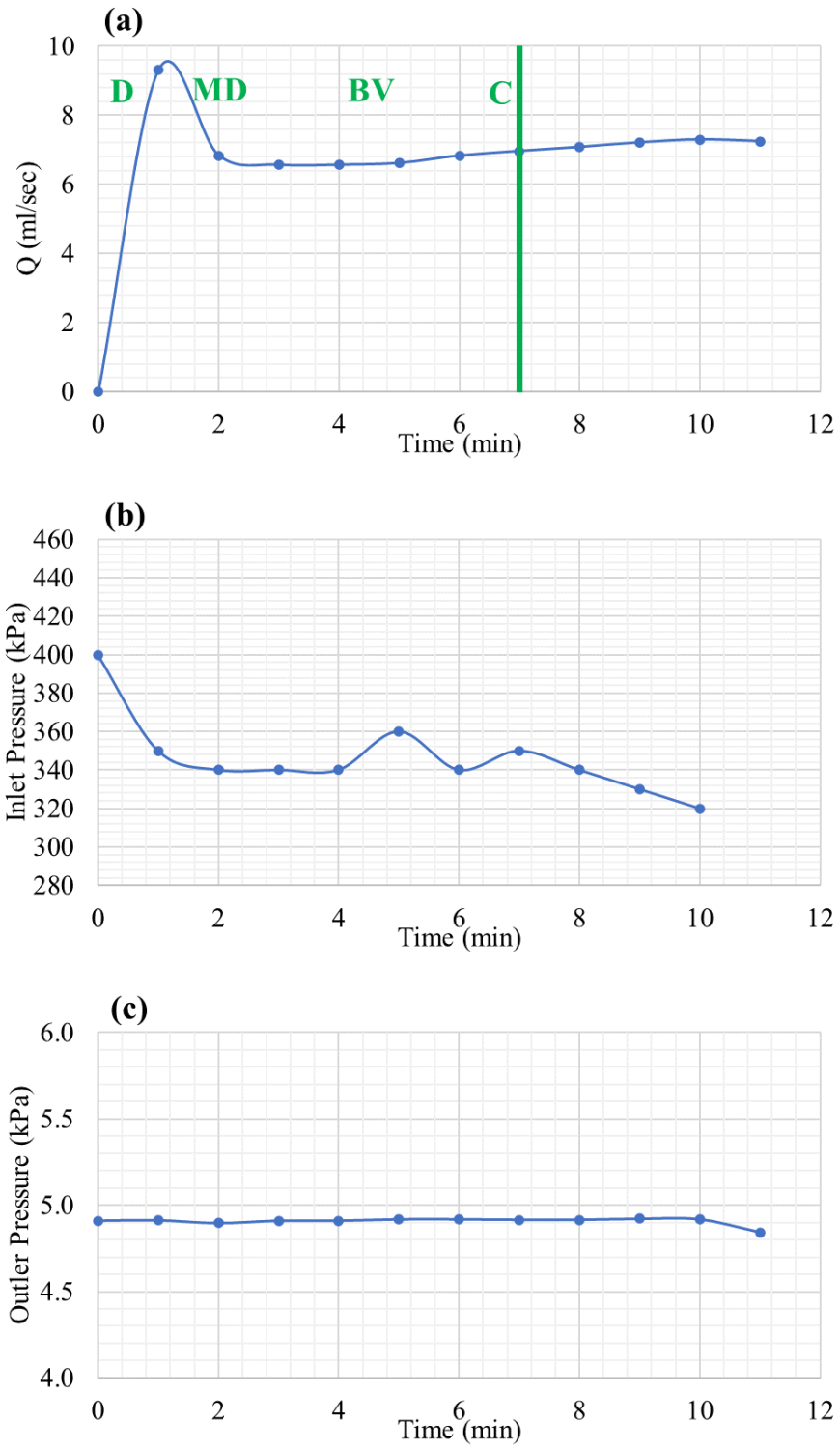

Figure 3.7 Change in (a) outflow rate, (b) inlet pressure, (c) outlet pressure, for the filter with FC of 0%

Figure 3.8 Change of water quality for the filter with FC of 0% (Source: Ecemis, 2023)

Figure 3.9 Final hole diameter (2 – 3 mm) for the filter with FC of 0% (Source: Ecemis, 2023)

3.3.2. Static Test for Fines Content of 2%

The second NEF test was performed on filter material that had 2% silt content. The same procedure in the first test was followed to prepare the samples. Then, 400 kPa pressure was applied (schematically shown in Figure 4.2). Clearwater was seen after 9 minutes with a 138 ml/min flow rate. The test was ended at the end of 10 minutes. Inlet pressure was not varied during the test, and the measured pressure in the outlet was around 4.76 kPa. When the hole diameter change was checked, it was seen that the change was

not changed compared to the initial diameter. The variation in outflow rate, measured pore water pressures at the inlet and the outlet are shown in Figure 3.10a-c, respectively. The change in water quality during the test and the final hole diameter are given in Figure 3.11 and Figure 3.12. Eventually, observing almost no change in the hole diameter, low outflow rate, and stable pressure in the pressure gauge, the filter material was decided as successful.

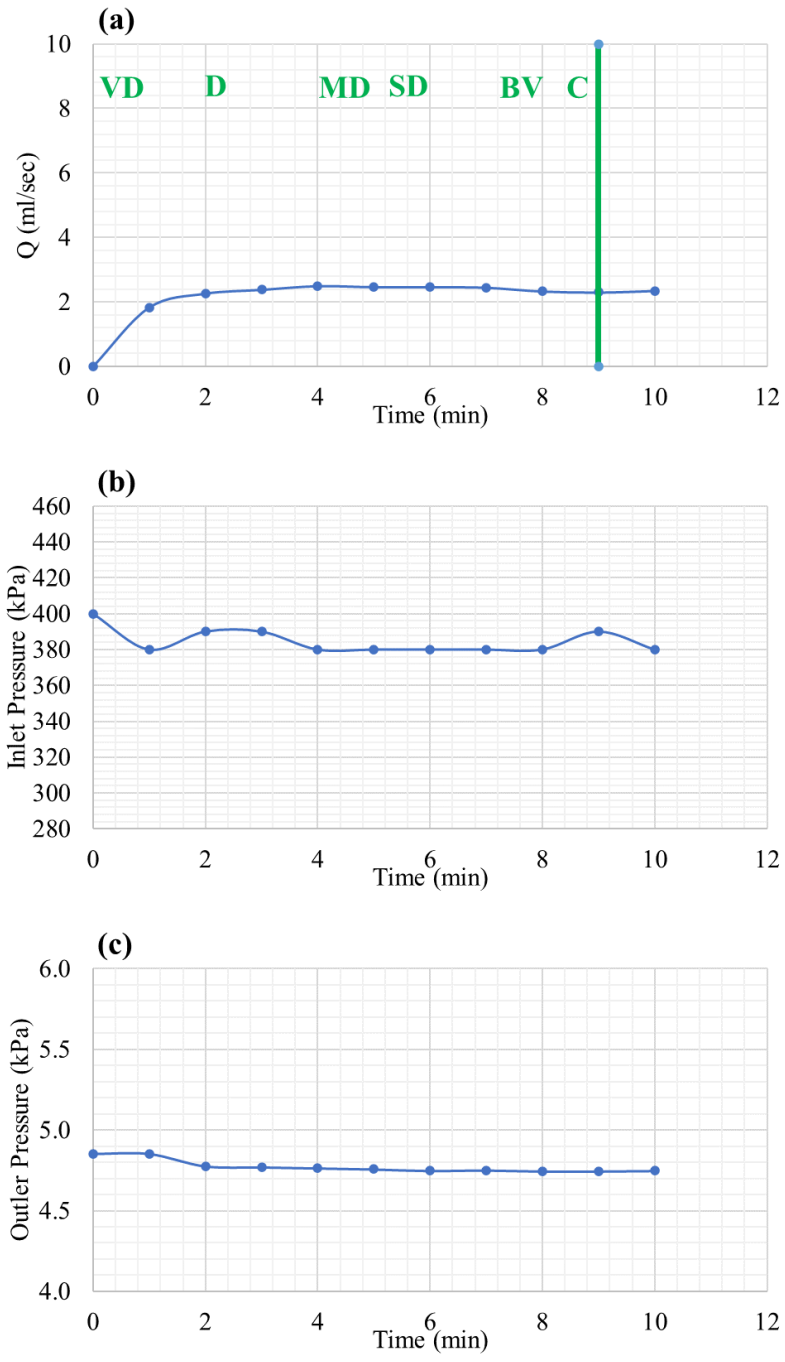

Figure 3.10 Change in (a) outflow rate, (b) inlet pressure, (c) outlet pressure, for the filter with FC of 2% (Source: Ecemis, 2023)

Figure 3.11 Change of water quality for the filter with FC of 2% (Source: Ecemis, 2023)

Figure 3.12 Final hole diameter (1 mm) for the filter with FC of 2% (Source: Ecemis, 2023)

3.3.3. Static Test for Fines Content of 5%

The last test of the static series was conducted on the filter material, which had 5% non-plastic silt content. The gravel, base, and filter samples were prepared and placed into the plexiglass cell. When the setup was completed, 400 kPa pore pressure was applied from the inlet of the apparatus (schematically shown in Figure 4.2). After 9 minutes, clearwater was observed with a constant flow rate of 95 ml/min, and the test was ended at 11 minutes. The inlet pressure remained at about 400 kPa during the test, and the outlet

pressure was recorded at around 4.65 kPa. Besides, the final diameter of the hole was the same as the initial diameter as shown in Figure 3.15. The change in outflow rate, inlet, and outlet pore water pressure; and the water quality during the test are demonstrated in Figure 3.13a-c, and Figure 3.14, respectively. In view of minor variations in the inlet pressure, low flow rate, and no change in hole diameter have shown that the filter material is successful.

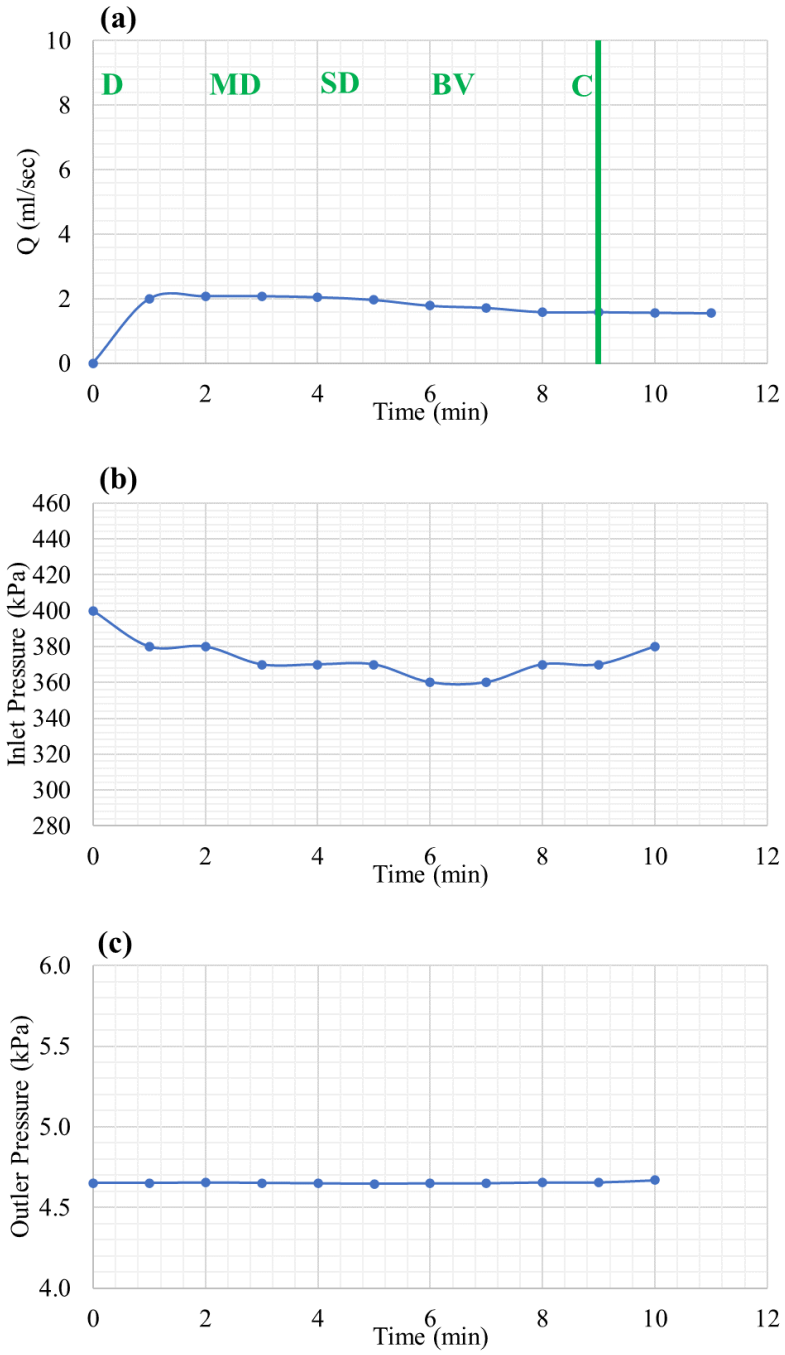

Figure 3.13 Change in (a) outflow rate, (b) inlet pressure, (c) outlet pressure, for the filter with FC of 5%

Figure 3.14 Change of water quality for the filter with FC of 5% (Source: Ecemis, 2023)

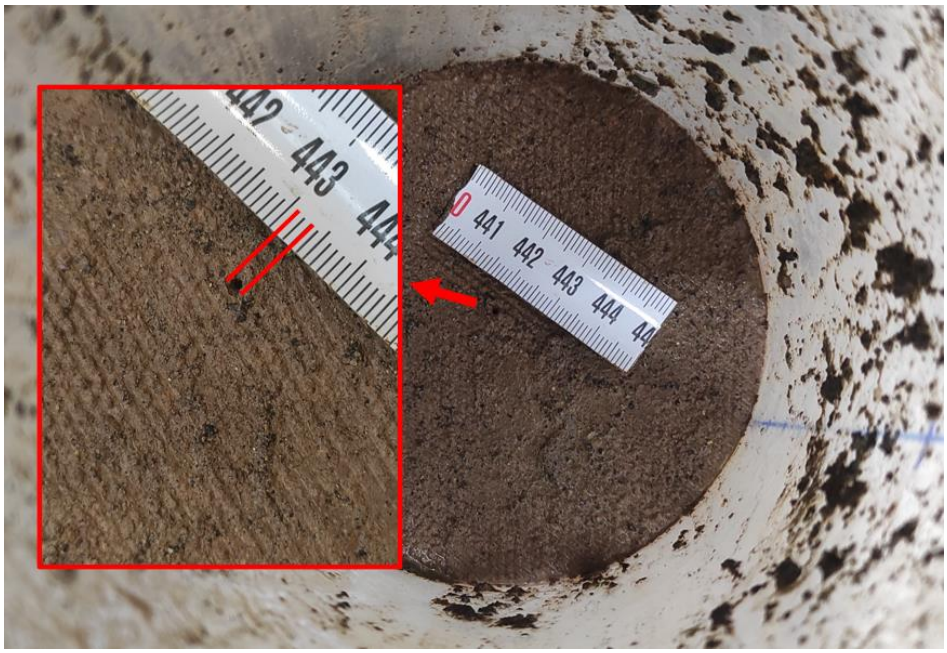

Figure 3.15 Final hole diameter (1 mm) for the filter with FC of 5% (Source: Ecemis, 2023)

3.4. Dynamic Tests

In the scope of dynamic tests, the frequency was the main variable. In the light of static NEF test results, including Rahmanlar Dam, filters containing 5% fines content demonstrated the best performance based on all results together. In these tests, the test apparatus was installed on the 1D shaking table, to which two submersible accelerometers (SAs) were attached. The shaking table and test apparatus are shown in Figure 3.16. Then,

the samples were prepared and placed by following the same procedure as the static tests. In the first 10 minutes, the static NEF test was performed. Then, sinusoidal excitation was applied to the apparatus. Maximum acceleration, a_{max} of excitation was 0.5g, and it was applied for 20 seconds for two different frequencies of 2Hz and 4Hz. The results and observations are detailed for each test in the following sections.

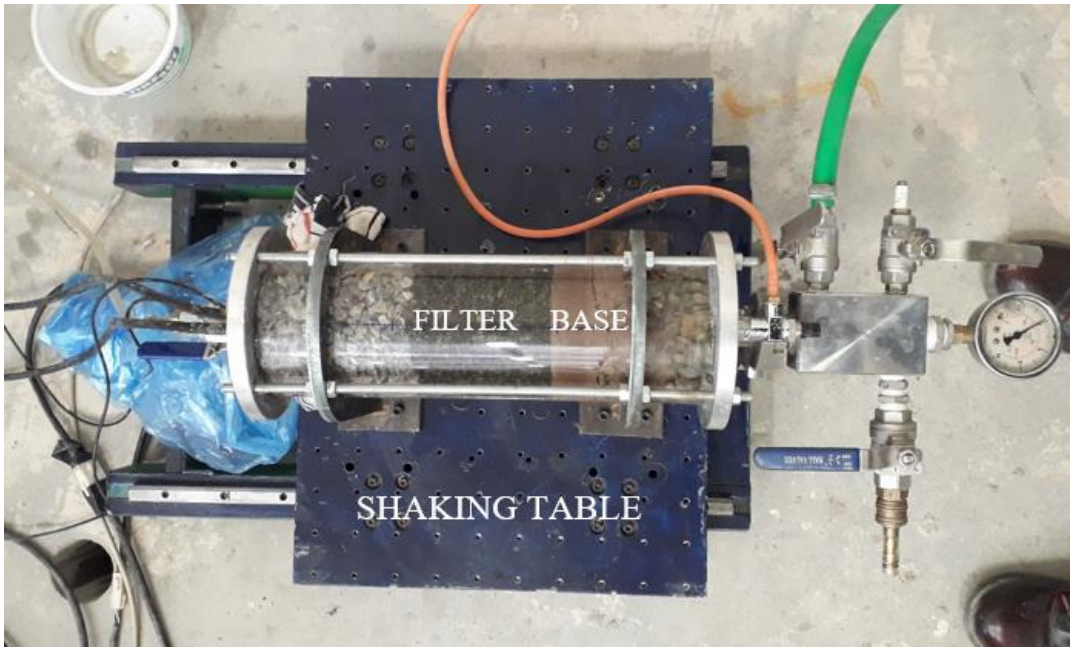

Figure 3.16 NEF Test attached to shaking table (Source: Ecemis, 2023)

The applied acceleration to the shaking table during the dynamic tests is shown in Figure 3.17a-b for frequencies of 2Hz, and 4Hz, respectively.

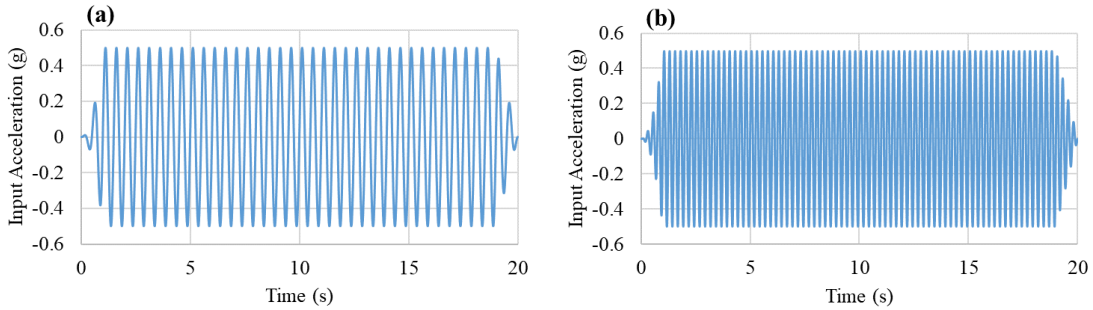

Figure 3.17 Input acceleration during sinusoidal excitations for frequencies of (a) 2Hz, and (b) 4Hz

3.4.1. Dynamic Test for 2Hz Frequency

The first test of the dynamic series was conducted for 2Hz frequency with 0.5g maximum acceleration, and the filter sample had 5% silt content. As aforementioned, the static test was carried out for the first 10 minutes, and the clearwater came out from the outlet with a flow rate of 104 ml/min. After the excitation was applied for 20 seconds, the outflow rate dropped, and clearwater was seen after 8 minutes with an 81 ml/min constant flow rate. However, at the beginning of the shaking, the outflow was high, and the inlet pressure decreased. Besides, the hole diameter was enlarged from 1 mm to 2 mm, as shown in Figure 3.20. The green line in the outflow rate represents the time clearwater was seen, and the red one is when dynamic excitation is applied. The change in Q, pore pressure at the inlet and at the outlet, and measured acceleration by SAs plots are given in Figure 3.18a-d. The green line in the outflow rate plot represents the time clearwater was seen, and the red one is when dynamic excitation was applied. Collected concentrated water during the test is shown in Figure 3.19. As a result, the filter material was evaluated as unsuccessful due to the enlargement of the hole diameter, sudden drop in inlet pressure, and seepage flow variations.

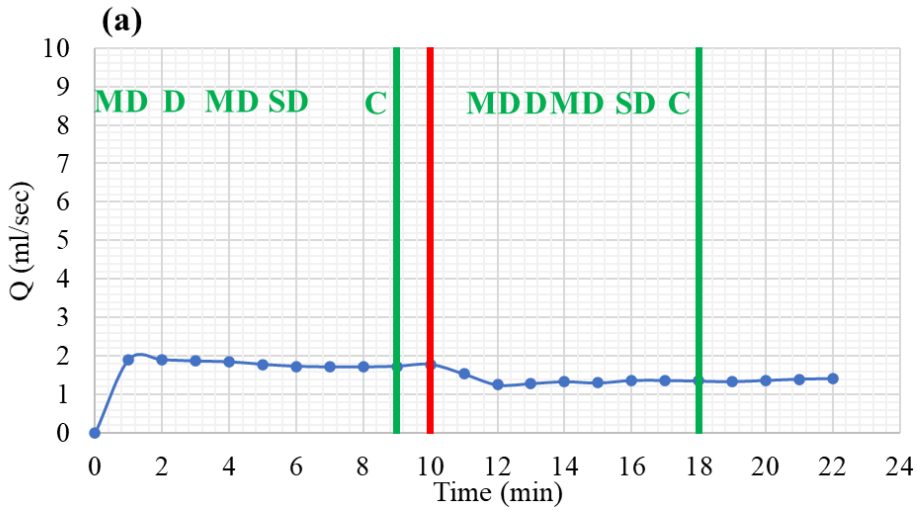

Figure 3.18 Change in (a) rate of flow, (b) inlet pressure, (c) outlet pressure, and (d) measured acceleration for 2Hz frequency dynamic test

(cont. on next page)

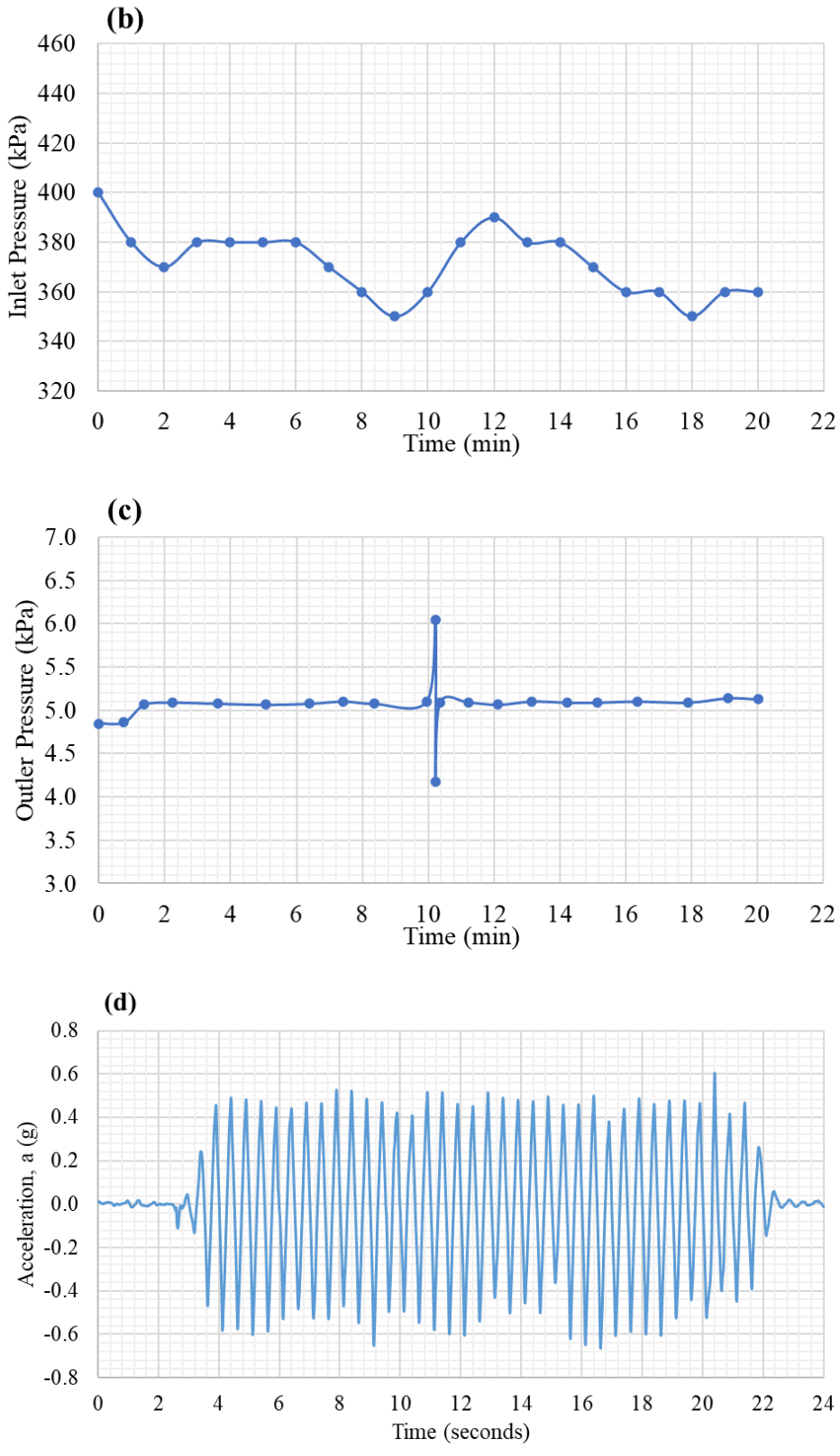

Figure 3.18 (cont.)

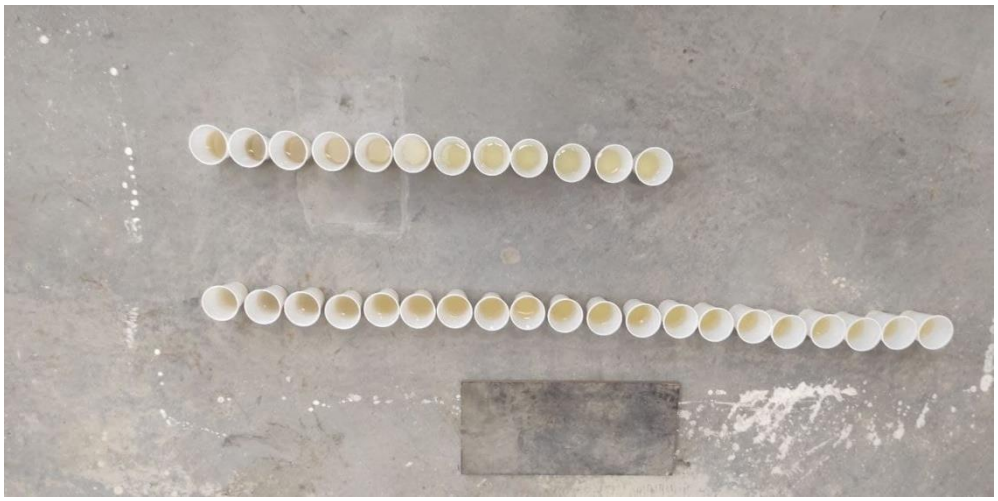

Figure 3.19 Change of water quality for 2Hz frequency dynamic test (Source: Ecemis, 2023)

Figure 3.20 Final hole diameter for 2Hz frequency dynamic test (Source: Ecemis, 2023)

3.4.2. Dynamic Test for 4Hz Frequency

The second dynamic test was carried out for 4Hz frequency. As the same with the first dynamic test, the silt content in the filter sample was 5%, and the maximum acceleration, a_{max}, 0.5g. Before the sinusoidal excitation, the static test procedure was followed, and clearwater was observed with a 135 ml/min constant outflow rate after 9 minutes. Then, the excitation was applied for 20 seconds, and with decreasing outflow

rate, 3 minutes later, clearwater came out with a 102 ml/min flow rate. The inlet pressure dropped due to high seepage flow at the beginning of the test, and then it remained nearly constant, whereas, after the excitation, it increased with a low outflow rate. The outlet pressure stabilized around 5 kPa with high variations, and the change in the hole diameter was measured from 1 mm to 3 mm, which is given in Figure 3.23. The variation in Q, inlet, and outlet pore pressures and measured acceleration by SAs are given inFigure 3.21a-d. The green line represents the time at which clearwater was observed, and the red line represents the time at which sinusoidal excitation was applied. Consequently, filter performance has been evaluated as unsuccessful due to the increase in the hole diameter, high outflow rate, and decrease in inlet pressure.

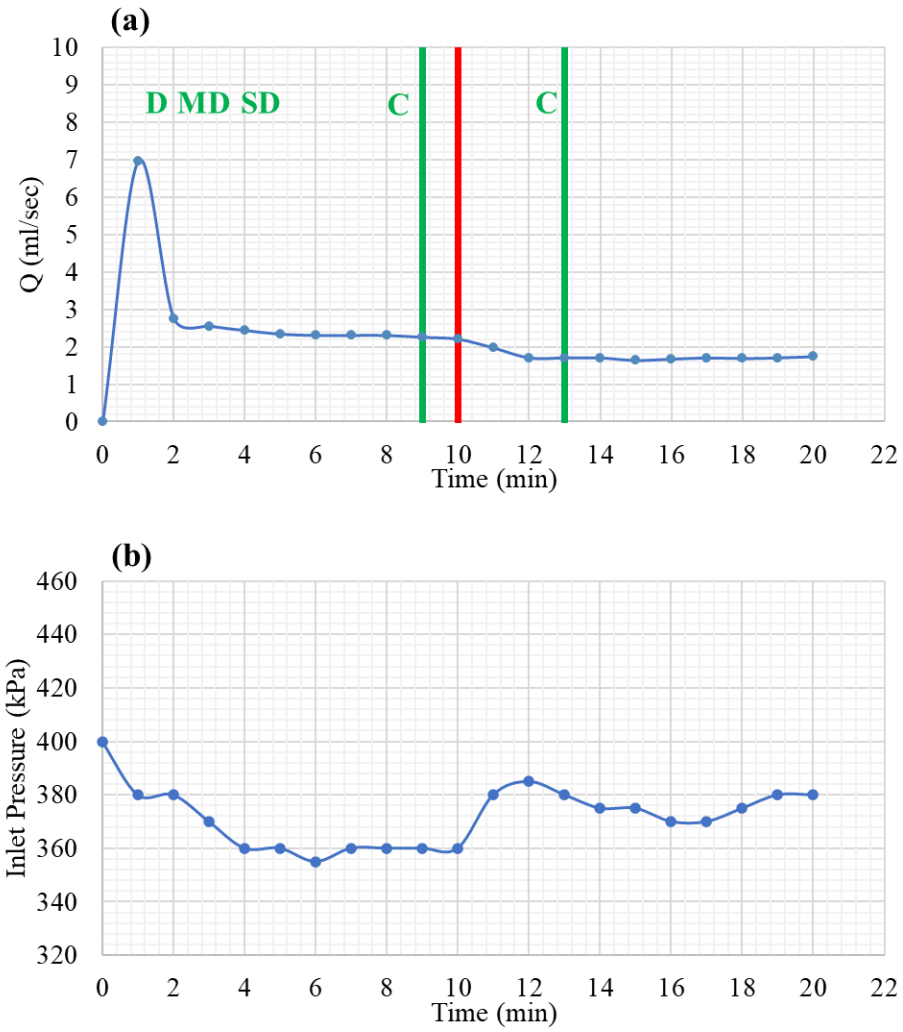

Figure 3.21 Change in (a) rate of flow, (b) inlet pressure, (c) outlet pressure, and (d) measured acceleration for 4Hz frequency dynamic test

(cont. on next page)

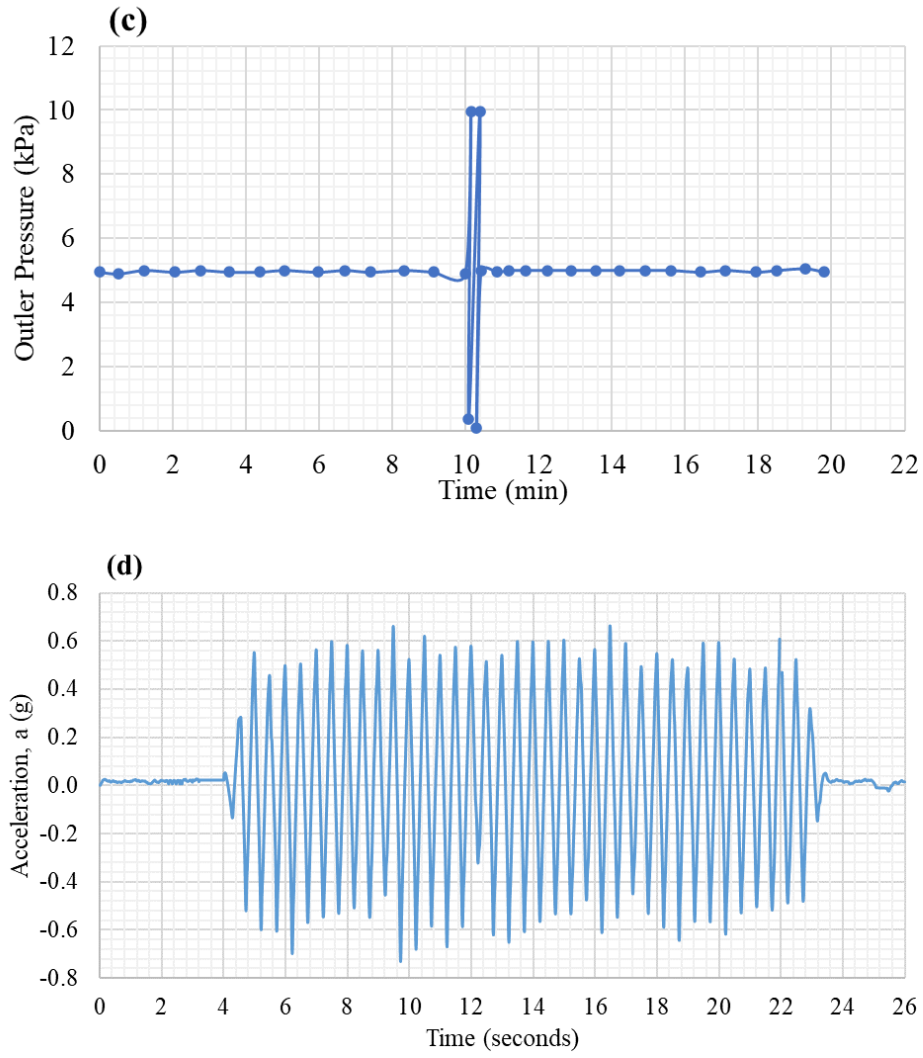

Figure 3.21 (cont.)

Figure 3.22 Change of water quality for 4Hz frequency dynamic test (Source: Ecemis, 2023)

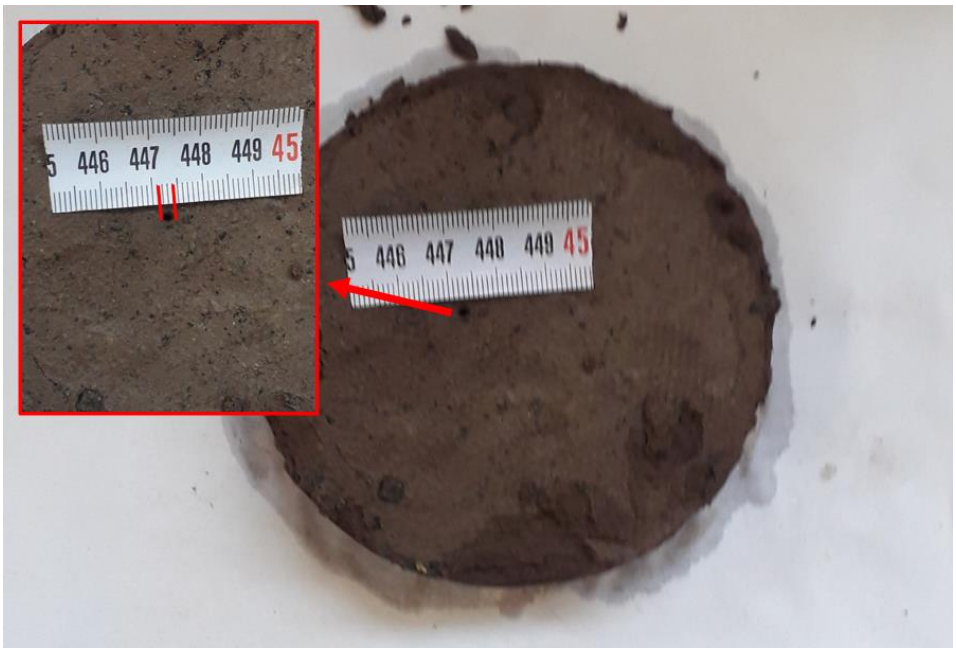

Figure 3.23 Final hole diameter for 4Hz frequency dynamic test (Source: Ecemis, 2023)

3.5. Summary of NEF Tests

In this section, all static and all dynamic tests are compared with each other, and an understanding of unsuccessful and successful filter behavior is provided. In Table 3.5, general information about the results of the NEF tests is summarized. In static tests, the filter with FC 0% is evaluated as unsuccessful, while the filters with FC of 2% and 5% are evaluated as successful. It is obvious that fines content increases internal erosion resistance. In dynamic tests, both tests with 2Hz and 4 Hz frequencies are evaluated as unsuccessful. Therefore, it is hard to comment on the frequency effect directly, but in the dynamic test with 4Hz frequency, the final hole diameter is larger than the test with 2Hz frequency. It can result that higher frequency increases erosion rate because the test duration is the same for both tests.

The compliance of the samples with the criterias of Sherard and Dunnigan (1989) and Foster and Fell (2001) are given in Table 3.6. It is seen that whereas all the filters satisfy the criteria of Foster and Fell, they do not meet the criteria of Sherard and Dunnigan. It means that the filter performance can be incompatible with the design criterias. For example, the filters with FC of 2% and 5% are successful, but they do not comply with Sherard and Dunnigan's criteria. Also, behavior under seismic loading is also unpredictable because the filter with FC of 5% is evaluated as successful under static

loading but unsuccessful under dynamic loading. For these reasons, the choice of filter in the design of embankment dams is important for safety.

When variations of Q values during the tests are compared, an increasing trend is observed in the outflow rate of the unsuccessful filter, which is the clean sand (Figure 3.24a). On the other hand, even if the dynamic test performed for 4Hz frequency has a stabilized outflow rate, the filter has been evaluated as unsuccessful (Figure 3.24b). Consequently, it can be understood from the results that enlargement of the preformed hole is evaluated as unsuccessful due to the loss of base materials.

Table 3.5 Summary of NEF tests

Fines Content (%)	Loading Condition	Frequency Hz	$\frac{(D_{15})_F}{(d_{85})_B}$	Final hole diameter (mm)	The trend of flow rate, Q	Water Quality	Evaluation
0	Static	-	3.3	2 ~ 3	Increasing	Clear	**Unsuccessful**
2	Static	-	2.9	1	Constant	Clear	**Successful**
5	Static	-	2.8	1	Constant	Clear	**Successful**
5	Dynamic	2	2.8	2	Increasing	Clear	**Unsuccessful**
5	Dynamic	4	2.8	2 ~ 3	Constant	Clear	**Unsuccessful**

Table 3.6 Compliance of samples to the criteria

Fines Content (%)	$(D_{15})_F$	$(d_{85})_B$	$\frac{(D_{15})_F}{(d_{85})_B}$	Sherard & Dunnigan (1989)	Foster & Fell (2001)
0	0.36	0.11	3.3	**NOT OK**	**OK**
2	0.32	0.11	2.9	**NOT OK**	**OK**
5	0.31	0.11	2.8	**NOT OK**	**OK**
5	0.31	0.11	2.8	**NOT OK**	**OK**
5	0.31	0.11	2.8	**NOT OK**	**OK**

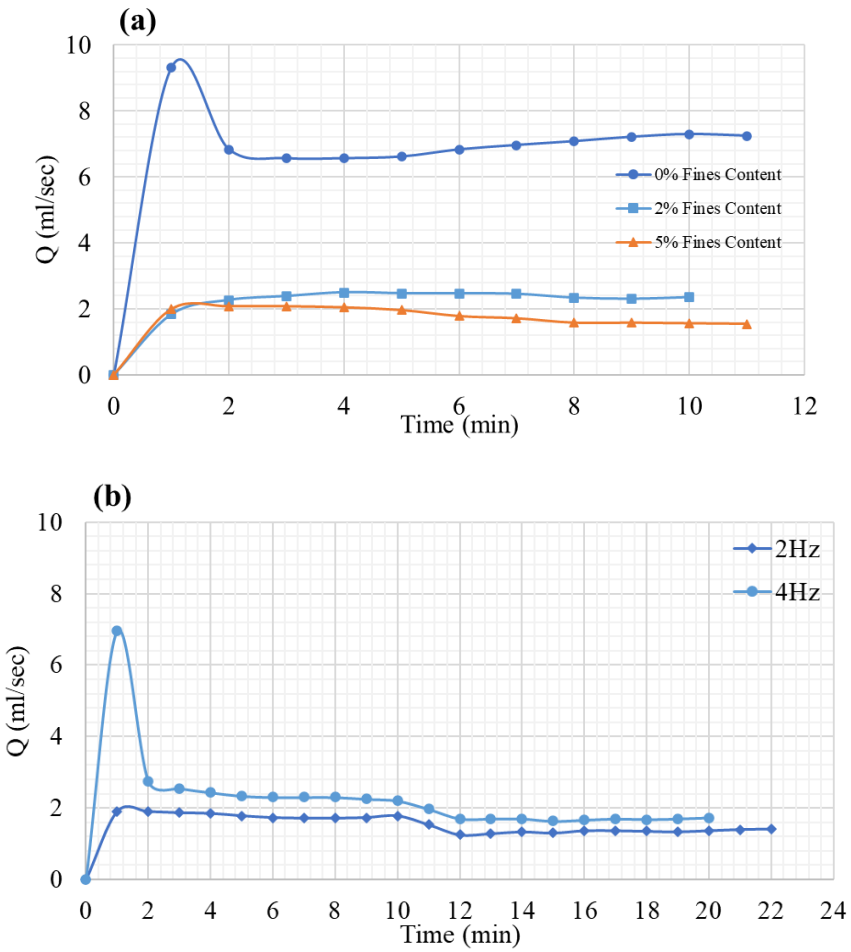

Figure 3.24 Variation in Q of (a) static tests, (b) dynamic tests

In the following chapter, numerical modeling of internal erosion in FLAC3D is given in detail. Fluid-mechanical interaction in FLAC3D, model geometry, boundary conditions, material models, and parameters are explained. After that, numerical results are given for each NEF test, and they are compared with the results of the NEF tests, which is already presented in this chapter.

CHAPTER 4

NUMERICAL MODELING OF INTERNAL EROSION

4.1. Introduction

In this chapter, internal erosion simulation is explained. First, examples using different analysis methods are given. After that, general information about FLAC3D 6.0 and its fluid-flow approach is summarized. Then, the numerical modeling of the NEF test in FLAC3D 6.0 is detailed. Geometry, boundary, and initial conditions of the model and material models, including fluid and constitutive models follow. Besides, the choice of parameters and theoretical approach of FLAC3D is clarified. Eventually, numerical results which are presented for each NEF test are given in CHAPTER 3.

4.2. Numerical Modeling of Internal Erosion

In the scope of the study, it is aimed to figure out the relationship between base and filter materials in embankment dams. The static and dynamic NEF test series mentioned in the previous chapter explains how fines content and frequency affect filter performance. In addition to laboratory effort, numerical modeling can also help it. However, modeling of internal erosion is complicated due to changes in properties of base materials, especially the outer side of the base body, the ability to erosion of not only finer materials but also coarser materials, widening of the pipe, slope stability effect, and others (Fread, 1991). Researchers have made many attempts using different approaches like FEM, DEM, CFD, FDM, SPH, and analytical.

Cividini and Gioda (2004) studied FEM modeling of internal erosion by implementing erosion law which takes into account the erosion rate. As a result, their model verified the erosion tests conducted in the lab. However, the change in permeability over time did not be considered.

Frishfelds et al. (2011) simulated the NEF test in CFD analysis, and prevention of base material erosion was observed in the models. On the other hand, the movement path

of particles was not as claimed by Sherard and Dunnigan's study. Figure 4.1a-b demonstrate the initial phase and transportation of base particles (finer).

Mercier (2014) modeled erosion behavior in cohesive soils in Ansys Fluent, which uses the CFD approach. The models are verified through Hole Erosion (HET) and JET Erosion (JET) tests. It is revealed that the model showed good performance in estimating erosion behavior even if the erosion parameters varied.

Xu and Zhang (2013) practiced the model using Excel VBA, and they tested their model on Teton Dam, which failed due to concentrated leak erosion. Since it proceeds progressively, the enlargement of the pipe increases depending on the erosion rate.

Rahimi and Shafieezahed (2020) modelled backward erosion piping in FLAC3D and examined its impact on the stability of the downstream slope of levees or dikes. They implemented that update in strength and stiffness properties depending on porosity change in eroded regions and used the permeability amplification factor. It has resulted that this hydro-mechanical coupled approach provides reliable design owing to observing higher safety values when ignorance.

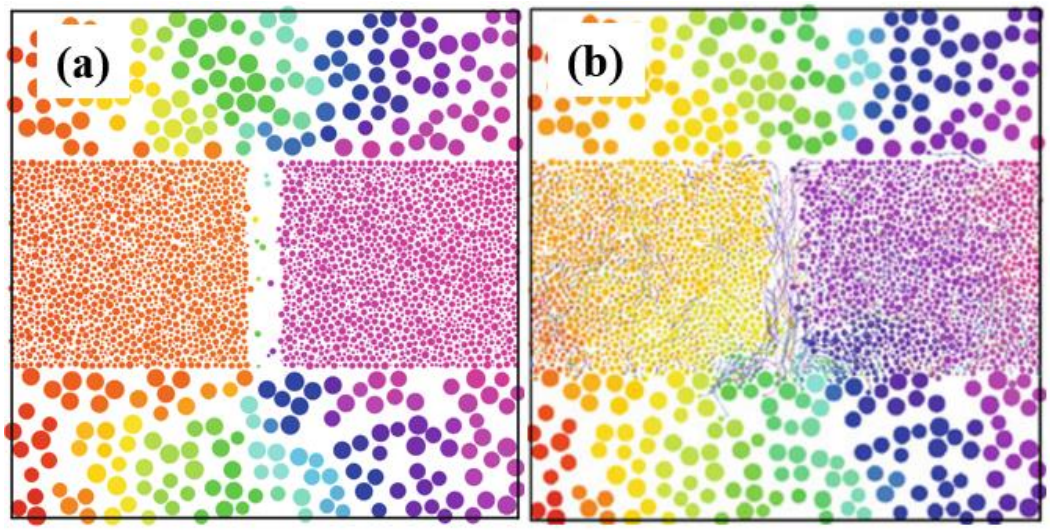

Figure 4.1 CFD analysis of NEF Tests performed by Frishfields et al. (2011) (a) initial phase, and (b) transportation of base particles into pores of the filter (Source: Frishfields et al., 2011)

Sun et al. (2021) used the coupled CFD-DEM approach, and they modeled the initiation, continuation, and progression phases of the soil erosion around piles. The effect of grading, pile-soil friction coefficient, density, and pile spacing on resistance have been investigated, and they detected the critical point at which internal erosion was initiated.

Ma et al. (2022) studied on SPH approach and modeled internal erosion in embankments. Their simulation showed good performance when verified with experiments. Besides, the reduction in strength parameters has been reached.

In this study, numerical modeling of the NEF test in FLAC3D is performed. The results are compared to the results of the tests carried out in the IZTECH laboratory in 2022 by Hadi Valizadeh. The details belonging to them are given in CHAPTER 3.

4.3. FLAC 3D

FLAC3D is a three-dimensional analysis program developed by ITASCA Consulting Group, Inc. Explicit Langrangian finite-volume method is used in engineering computations. Modeling of the materials is provided as polyhedral elements in a three-dimensional (3D) grid. The software offers the yielding, flow, deformation, and movement of the elements.

It is chosen for having the ability to model fluid flow in permeable soil and to analyze flow and mechanical. By remembering that goal is to understand the relationship between filter and base materials, it is practical to use FLAC3D for fluid and solid interaction. The fluid flow and mechanical process of the problem are solved together by coupling. Biot's theory is applicable in coupled analysis, and it is applied to the model by Biot coefficient, α. Besides, pore-pressure generation can be completed in dynamic loading conditions.

4.3.1. Fluid-Mechanical Interaction in FLAC3D

FLAC3D allows users to simulate the flow of water through porous materials for both flow-only and coupling with mechanical calculations. The coupling mechanism is the exact consolidation process which includes the variation of effective stress and the behavior of fluid when the deformation of volume due to pore pressure change. The options for constitutive models are valid for not only permeable or impermeable materials but also isotropic and anisotropic materials.

4.4. NEF Test Modeling

The configuration of the NEF test and material boundaries are shown in Figure 4.2. When 400 kPa pore pressure is applied from the inlet part (left-hand side), the valve (right-hand side) is opened to let the water go out of the apparatus during the test. The numerical model was set based on the configuration given in the figure. At first, two stages for static tests and three stages for dynamic tests were identified as listed below:

(1) Initial stage

(2) Application of pore pressure from the inlet part of the model (static tests)

(3) Application of sinusoidal loading (dynamic tests)

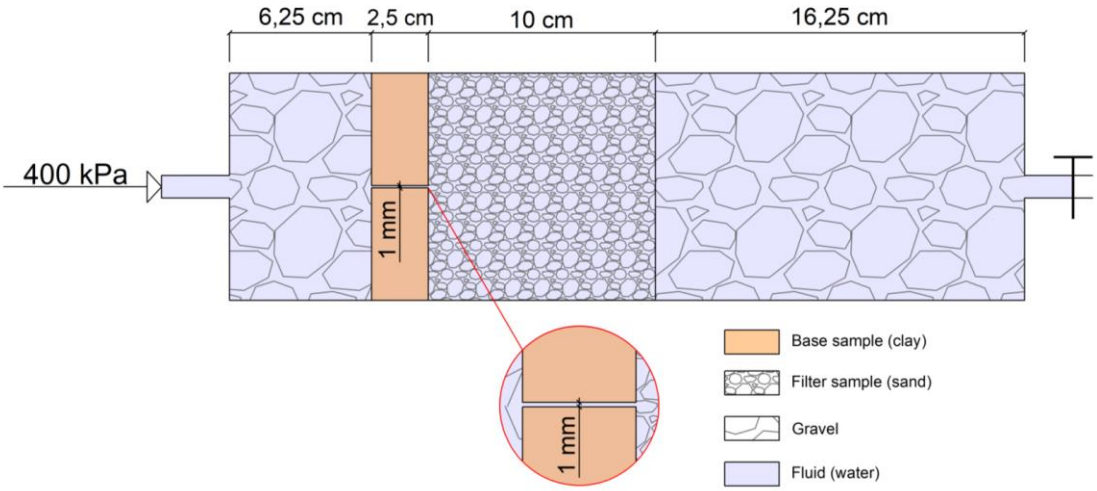

Figure 4.2 Configuration of NEF test used in the numerical models

4.4.1. Model Geometry

When it was decided to numerical modeling of NEF tests by a finite difference approach, FLAC was the first thought to choose. Due to being a cylindrical model, axisymmetric analysis seemed proper. However, FLAC only let the model axisymmetrically around the y-axis, and the test was conducted horizontally (Itasca Consulting Group, Inc., 2016). In this case, the effect of gravity cannot be taken into account, and the direction of gravity is also in the vertical direction. For these reasons, 3D analysis has been decided on the FLAC software.

The view of geometry is shown in Figure 4.3. There are 1428 zone (mesh elements) in the model. To represent the created hole in the base sample (pink-colored), a null model was considered, which is for removed or excavated region, but it was revealed that it is valid for impermeable materials. In the end, the grid configuration in that region was decided, as shown in Figure 4.4. However, because the fluid-mechanical interaction is critical in the analyses, different staging was conducted based on the coupling process. The details are given in the following sections.

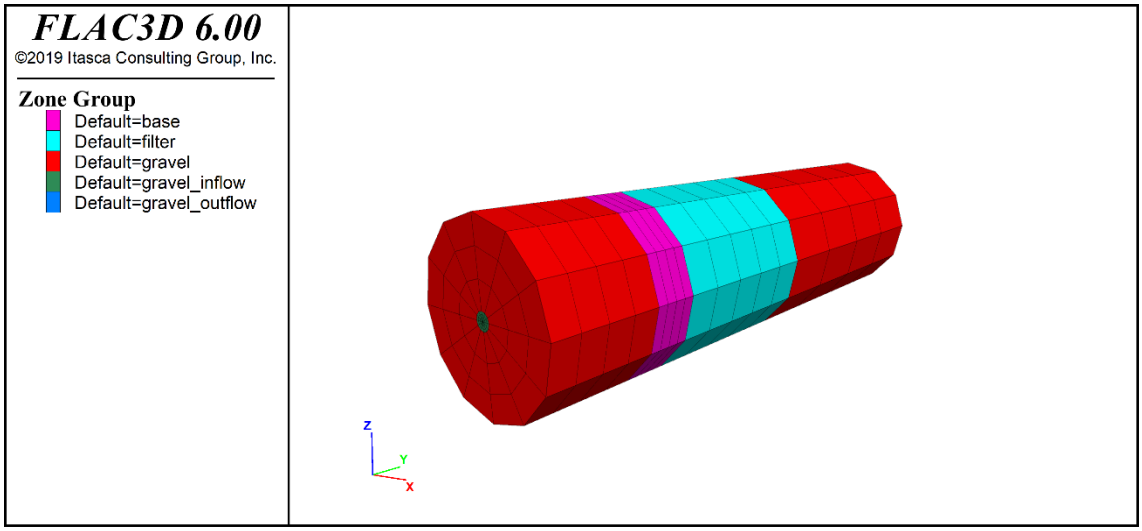

Figure 4.3 3D view of the NEF model geometry

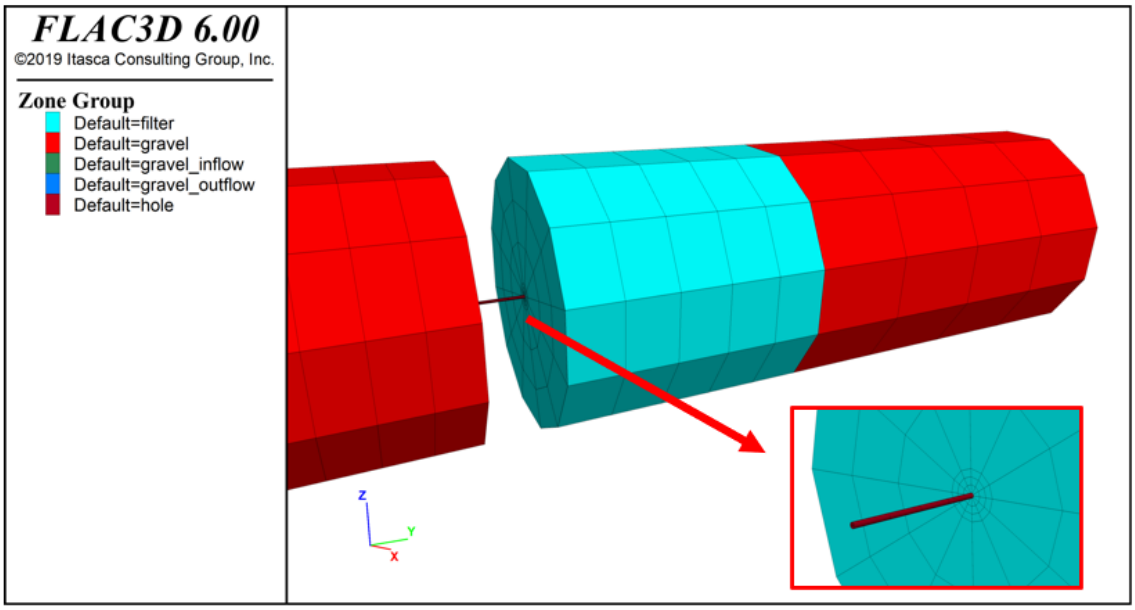

Figure 4.4 Created hole model in the base sample

4.4.2. Initial and Boundary Conditions

Fluid-flow boundary conditions and displacement boundary conditions differ in FLAC3D. In all grid points, roller support was defined in all stages, but only in the initial stage the grid points at the top of the model were released.

To specify fluid-flow boundary conditions is one of the challenges in modeling. Al boundaries are accepted as impermeable in the case of "free", which means that there is no flow between the grid and outside (Itasca Consulting Group, Inc., 2017). However, flow exchange is needed for NEF modeling, so 1-cm-diameter circular faces were created at the inlet and outlet faces of the model aimed to create permeable boundaries. After that, 400 kPa pore pressure was applied from the inflow face, and 0 kPa pore pressure was defined at the outflow face so that water left the grid from it (Sun et al., 2022).

4.4.3. Material Used in the Models

The strength and flow parameters of the materials were decided based on the laboratory test results given in CHAPTER 3. The accepted correlations were used to estimate the parameters for unavailable soil data, such as the permeability of base and gravel materials.

4.4.3.1. Fluid Model Parameters

The options for the fluid model were chosen isotropic for the filter, gravel, and hole; anisotropic for the base. Porosity, permeability, Biot coefficient, and Biot modulus were defined for each group.

Porosity values of base and filter materials were calculated by using laboratory data from relationships between index properties which are e, n, D_r, G_s, S, and w. The porosities for base and filter materials were 0.32 and 0.26, respectively. The porosity value is reduced gradually for filter materials consisting of 2% and 5% fine particles. The porosity value of gravel ranges between 0.25 – 0.40 (Hao et al., 2008), so it was chosen as 0.4 to let water flow more manageable. On the other hand, the porosity of the hole is taken as 1.

According to the Regulations for Earthworks and Natural Construction Materials published by State Hydraulic Works (Devlet Su İşleri, DSİ), the maximum hydraulic

conductivity of impermeable base material should be 10^{-7} cm/s. Permeable material (gravel) permeability should be larger than 10^{-4} cm/s; and the hydraulic conductivity of semi-impermeable filter material should be between 10^{-4} – 10^{-6} cm/s which was obtained as 1.12 x 10^{-3} in the constant head tests. As it was mentioned, base clay is defined as anisotropic material in which horizontal and vertical permeabilities differ from each other. It is suggested that horizontal permeability can be assumed to be ten times greater than vertical permeability (Fanchi, 2010). To specify the permeability of the hole was checked in the FLAC3D manual to see any maximum value for the permeability. However, it has been seen that there is no limit value for the permeability, so it started with values the same as gravel, and it was increased until the analysis gave unreasonable pore pressure contours.

There is no measurement of permeability for filter samples with fines. Hence, using correlations in the literature such as Hazen, Slichter, Kozeny-Carman, and Chapius (Cabalar & Akbulut, 2016; Chandel & Shankar, 2021), permeability values of the filters that have 2% and 5% fines content were calculated. The correlations for hydraulic conductivity are given in Table 4.1.

Table 4.1 Correlations for hydraulic conductivity

Researcher	Correlation	β
Hazen in 1892	$k = \frac{g}{\vartheta}\beta[1 + 10(n - 0.26)]D_{10}^2$	6 x 10^{-4}
Slichter in 1899	$k = \frac{g}{\vartheta}\beta n^{3.287} D_{10}^2$	10^{-2}
Kozeny-Carman in 1956	$k = \frac{g}{\vartheta}\beta \left[\frac{n^3}{(1-n)^2}\right] D_{10}^2$	8.3 x 10^{-3}
Chapuis et al. in 2005	$k = \beta \left[\frac{n^{2.35}}{(1-n)^{1.565}}\right] D_{10}^{1.565}$	1.412

υ: kinematic viscosity, β: sorting coefficient

After the definition of permeability and porosity values, the mobility coefficient and Biot parameters are estimated. The mobility coefficient is used instead of permeability in FLAC3D, which is the coefficient of the pressure term in Darcy's law. It is calculated as below:

$$k = \frac{k_h}{\rho_w g} \quad m^2/(Pa/sec) \tag{4.1}$$

where ρ_f is the density of fluid and g is the gravitational acceleration, and k_h is hydraulic conductivity.

The Biot coefficient, α, is the measure of how much fluid volume changes in a material element compared to the change in volume of the element's pores when the pore pressure changes. Biot coefficient of the materials generally ranges between 3n/(2+n) and 1. When a solid constituent is incompressible, Biot coefficient is 1. However, in that case, the materials were accepted as compressible. Whereas Biot coefficient depends on porosity, Biot modulus, M, depends on porosity, Biot coefficient, fluid, and solid bulk modulus:

$$M = \frac{K_f}{n+(\alpha-n)(1-\alpha)K_w/K} \tag{4.2}$$

where, K_w and K are bulk modulus for fluid and soil, respectively. Bulk modulus of water is 2 GPa at room temperature. However, a large modulus decelerates the calculation, so it is recommended to reduce K_w. Regarding the upper limit given below, the smallest value calculated for fluid bulk modulus is around 34 Pa.

$$K_w \leq 20n(K + \frac{4}{3}G) \tag{4.3}$$

The fluid model parameters used in the analyses are summarized in Table 2.1. Biot modulus values are given in the following section.

Table 4.2 Fluid model properties for materials

Zone	Material Model	n	k_v	k_v	k_h	k_h	α
			cm/s	m^2/(Pa sec)	cm/s	m^2/(Pa sec)	
Hole	Isotropic	1.00	1.00E+05	1.02E-01	-	-	1.00
Gravel	Isotropic	0.40	1.00E+02	1.02E-04	-	-	0.50
Base clay	Anisotropic	0.32	1.00E-07	1.02E-13	1.00E-06	1.02E-12	0.41
Filter sand without fine particles	Isotropic	0.26	1.12E-03	1.14E-09	-	-	0.35
Filter sand with 2% fine particles	Isotropic	0.25	6.41E-04	6.53E-10	-	-	0.33
Filter sand with 5% fine particles	Isotropic	0.24	5.23E-04	5.33E-10	-	-	0.32

4.4.3.2. Strength Parameters

In the scope of this study, it is aimed that the deformations are caused by fluid flow. However, strength parameters gain importance in erosion behavior. Two hydraulic criteria are defined by Fell et al. (2014). Based on the concentrated leak erosion mechanism, the stress applied to the soil around by water flow in the existent crack in the base of the dam should be greater than the sum of the tensile strength and the minor principal total stress of the soil as shown below:

$$\gamma_w h \geq \sigma_t + \sigma_3 \quad (4.4)$$

where (γ_wh) is the pore water pressure at the depth, σ_3 is the minor principal total stress, and σ_t is the tensile strength of the soil. Besides, the water flow velocity should be adequate to move detached particles (Figure 4.5).

FLAC3D serves many options for constitutive models classified as a null model, elastic model, and plastic model groups. In this study, Mohr-Coulomb is used. Mohr-Coulomb parameters of the base material are taken as the study of He et al. (2021), in which cracking in embankment dams has been simulated. For the other materials, Mohr-Coulomb model parameters are defined based on the approach to mathematical optimization of Vahdati (2014). When it came to the hole parameters, the same procedure was followed, and the strength parameters were decreased until getting reasonable results in initial conditions. The strength parameters (c, ϕ, E) for the Mohr-Coulomb material model are summarized in Table 4.3. Also, the calculated Biot modulus by using soil, fluid bulk modulus, and porosity values are given.

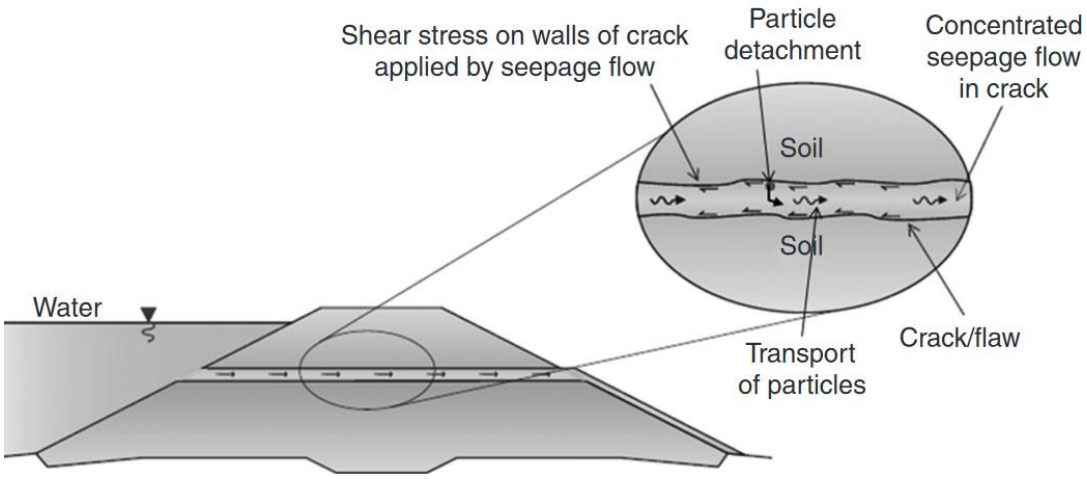

Figure 4.5 Concentrated leak erosion mechanism (Source: Fell et al., 2014)

Table 4.3 Mohr-Coulomb material properties used in numerical analyses

Zone	Material Model	γ_s kN/m^3	ν'	E' MPa	c' kPa	ϕ' (°)	M Pa
Hole	Mohr-Coulomb	0.1	0.49	10^{-7}	0	0	34
Gravel	Mohr-Coulomb	23.0	0.33	70	0	34	86
Base clay	Mohr-Coulomb	22.0	0.35	8	10	25	107
Filter sand without fine particles	Mohr-Coulomb	22.0	0.33	45	0	32	132
Filter sand with 2% fine particles	Mohr-Coulomb	22.0	0.33	45	0	32	137
Filter sand with 5% fine particles	Mohr-Coulomb	22.0	0.33	45	0	32	143

4.4.4. Dynamic Loading

Dynamic tests in the laboratory were conducted by applying sinusoidal excitation to the test apparatus for 20 seconds, with 0.5g a_{max} for two different frequencies of 2Hz and 4Hz (Figure 3.17). However, the numerical modeling of dynamic NEF tests has not been performed due to the restrictions of the boundary and the material models.

FLAC3D offers viscous (quiet) and free-field boundaries which prevent wave reflections in the numerical models. However, free-field boundary conditions are applicable for horizontal base. In future research, boundary problems in dynamic modeling should be considered.

4.5. Results of Static Numerical Models

In order to validate the numerical results, the results of the numerical models are checked with the experimental measurements. The validated parameters were the outflow rate (Q) and the change in hole diameter. The pore water pressure was also measured during the tests; however, it was not used in the verification of the numerical results due to calibration problems and fluctuation signals during laboratory work. In this section, numerical results are compared with not only NEF Tests performed in IZTECH but also other NEF Test results in numerical models in the literature.

The experiment series of NEF and CEF (Continuing Erosion Filter) were performed by Dam Safety Office in 2004 on the samples of Horsetooth, Teton, Tracey Fish Screen, and Many Farms Dams. NEF Test results are compared based on the closest particle size distribution to Kalabak Dam, which are Horsetooth Filter #3 and Many Farms Dam Filter #3 and Filter #4. The outflow and pore pressure results of these tests are shown in Figure 4.6a-b.

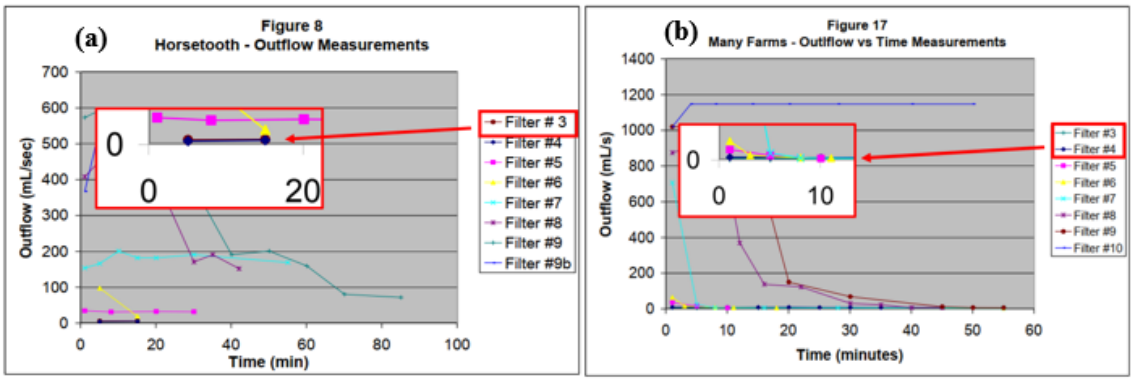

Figure 4.6 Outflow results of NEF tests conducted on (a) Horsetooth and (b) Many Farms Dams samples (Source: Dam Safety Office, 2004)

To simply the comparison of experimental and numerical results together, experimental tests are named as given in Table 4.4 below.

Table 4.4 Test names performed in the lab

Static tests performed in the lab	
Test Name	FC of the filter (%)
ST-1	0
ST-2	2
ST-3	5

4.5.1. Numerical Model Results of Static Test without Fine Particles in the Filter

The numerical model given in this section belongs to the ST-1 test (Table 4.4). Pore water pressure distribution, discharge vectors, and displacement of the hole are shown in Figure 4.7a-c. The unit of pore pressure values is in Pa; discharge vectors are in m/s, and displacements are in m. The applied pore pressure to the model is 400 kPa in the positive-y direction. The time is taken the same as the NEF tests performed in the lab. The duration of the ST-1 test is 11 minutes, so the model is run for 11 minutes.

It is seen from the figure that pore water pressure is decreased when it comes to the base material. However, the discharge through the preformed hole in the base sample is the highest. It shows that applied pore water pressure goes through the gravel material and then continues through the hole. When the high pressurized water goes through the hole, it causes the displacement in the walls of the hole in the same direction as pore pressure application. After that, the water arrives to the filter material and outlet gravel

material. Finally, it leaves the system from the outlet. The flow of water through the model is consistent with the flow of water through the NEF apparatus during the test.

In addition to the results of pore pressure distribution, discharge vectors and, displacement of the hole, outflow rate, Q is recorded during the analysis to compare numerical results with the experimental results. When Q values of the numerical model and experiment performed in the laboratory are plotted in the same graph (Figure 4.8), it is seen that numerical results do not show the same behavior as the results of the test. Besides, numerical results are 10^8 times smaller than experimental results.

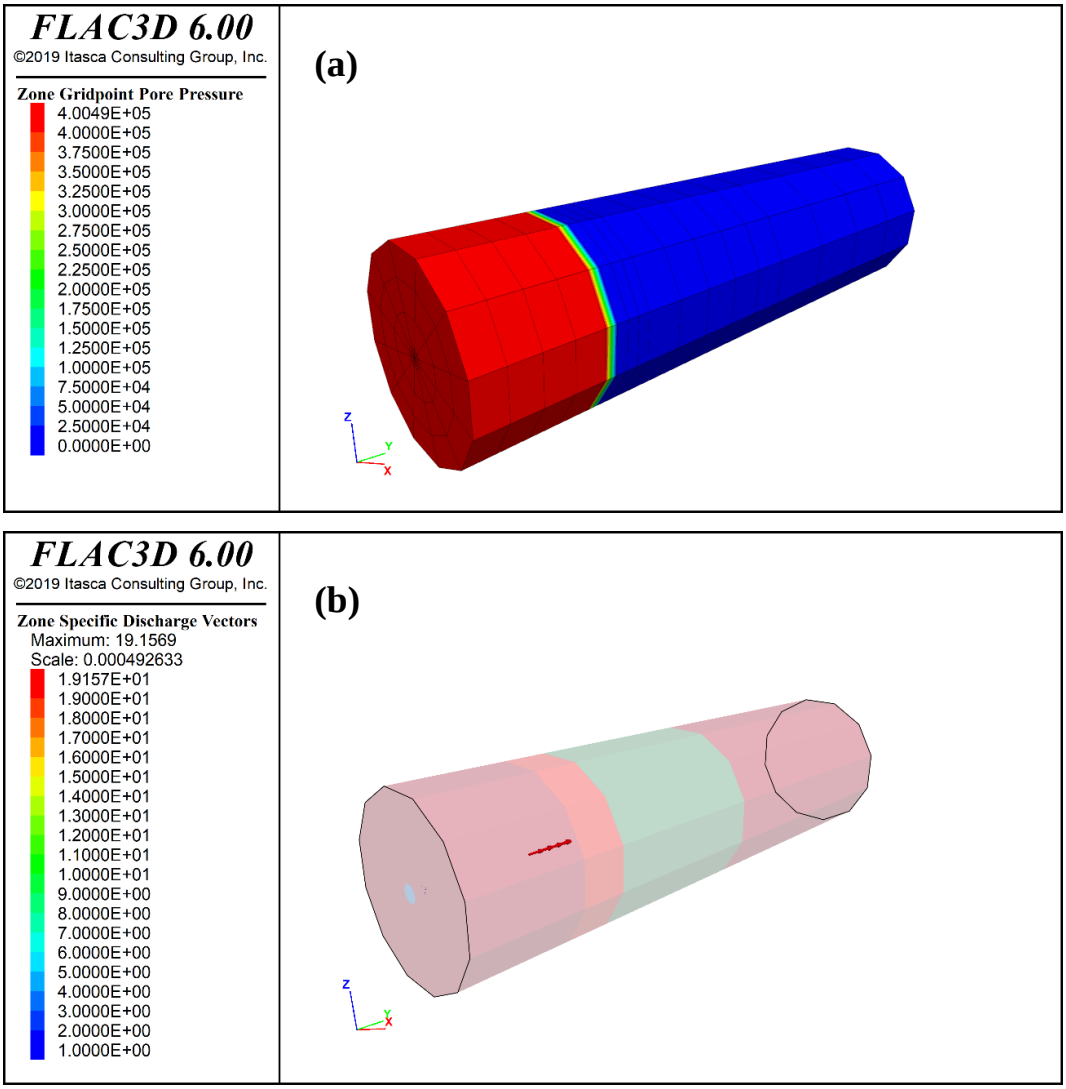

Figure 4.7 Numerical results of (a) Pore pressure distribution, (b) specific discharge and (c) hole displacement vectors, of the static test without fine particles in the filter

(cont. on next page)

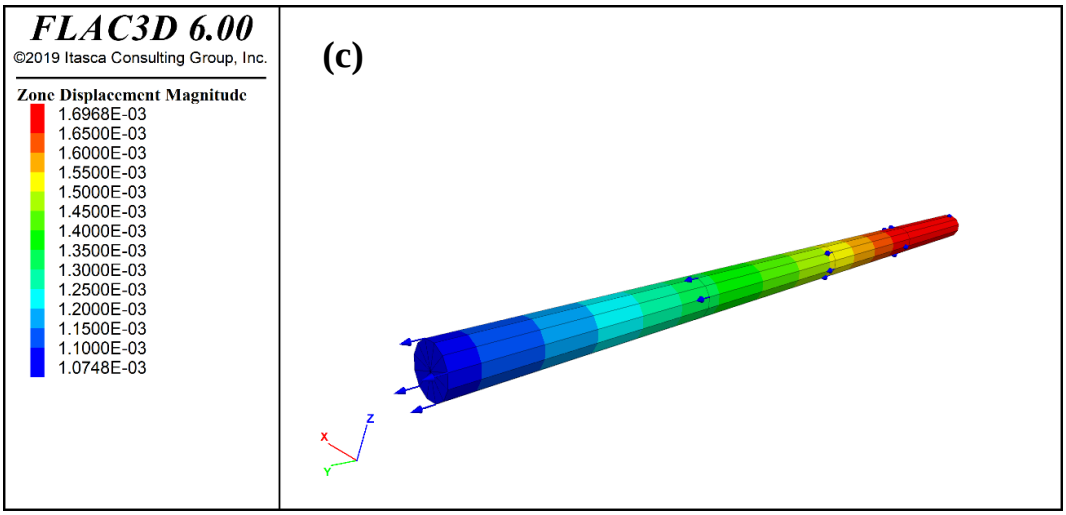

Figure 4.7 (cont.)

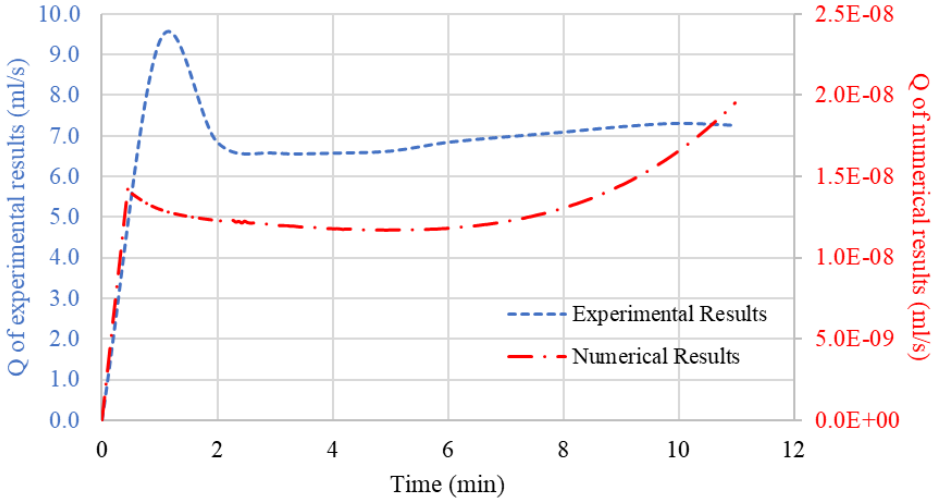

Figure 4.8 Comparison of outflow rates, Q of experimental (blue) and numerical (red) results for ST-1

4.5.2. Numerical Model Results of Static Test with 2% Fines Content in the Filter

The results of the static NEF test named ST-2 (Table 4.4) are presented in this section. Pore water pressure distribution, discharge vectors, and displacement of the hole are demonstrated in Figure 4.9a-c. The unit of pore pressure values is in Pa; discharge vectors are in m/s, and displacements are in m. 400 kPa pore pressure is applied to the model in positive-y direction, which is the inlet part of the model. The duration of ST-2 test in the laboratory is 10 minutes, so the model is analyzed for 10 minutes.

The water follows the same way as the numerical model of ST-1 explained in the previous chapter. It can be seen that pore pressure and displacement results are the same with the results of ST-1, as well. However, discharge vectors are smaller in ST-2 model. To remember, the filter of ST-1 is evaluated as unsuccessful in the static tests (Table 3.5), and the filter of ST-2 is successful. Therefore, it results in a smaller value of hydraulic gradient which is expected due to successful filter that can mitigate the internal erosion (Robbins, 2016).

The plot of the recorded Q values for the numerical model and the Q values of the experimental study for the ST-2 test is demonstrated in Figure 4.10. The trend of the results is similar to each other after the first 3 minutes due to stabilizing. However, numerical results are smaller 10^9 times than experimental results.

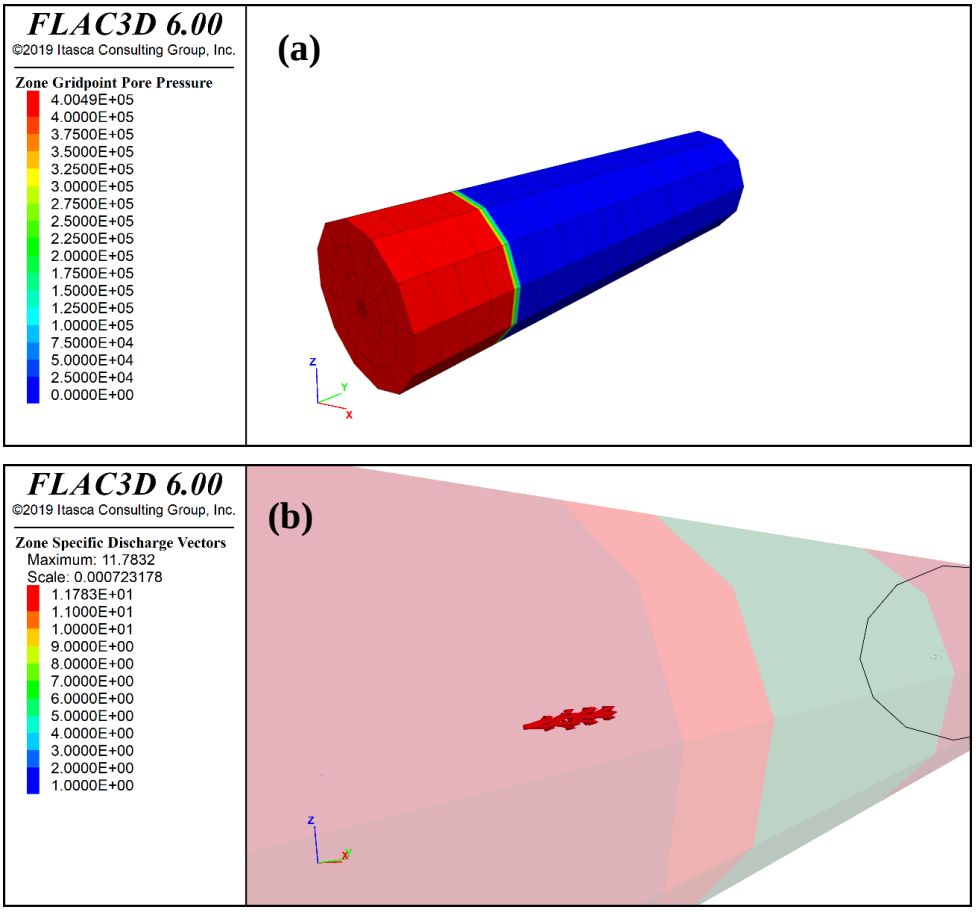

Figure 4.9 Numerical results of (a) Pore pressure distribution, (b) specific discharge vectors, (c) hole displacement vectors, of the static test with 2% fines content in the filter

(cont. on next page)

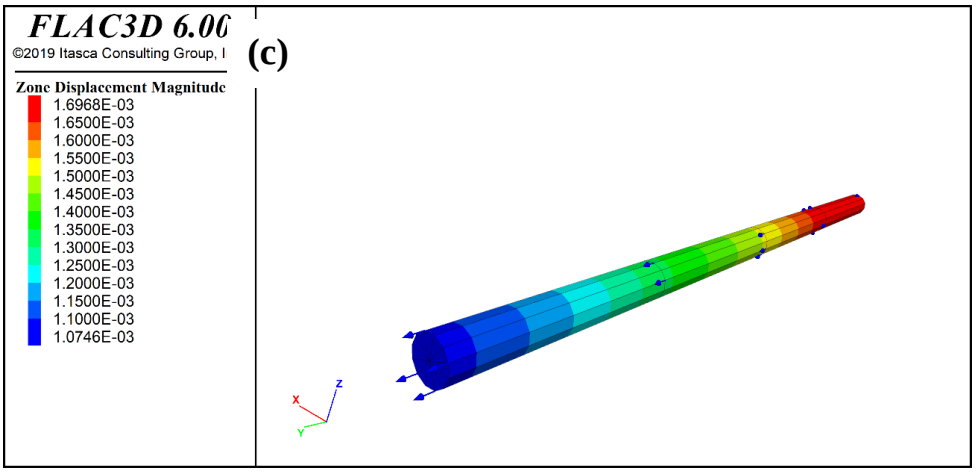

Figure 4.9 (cont.)

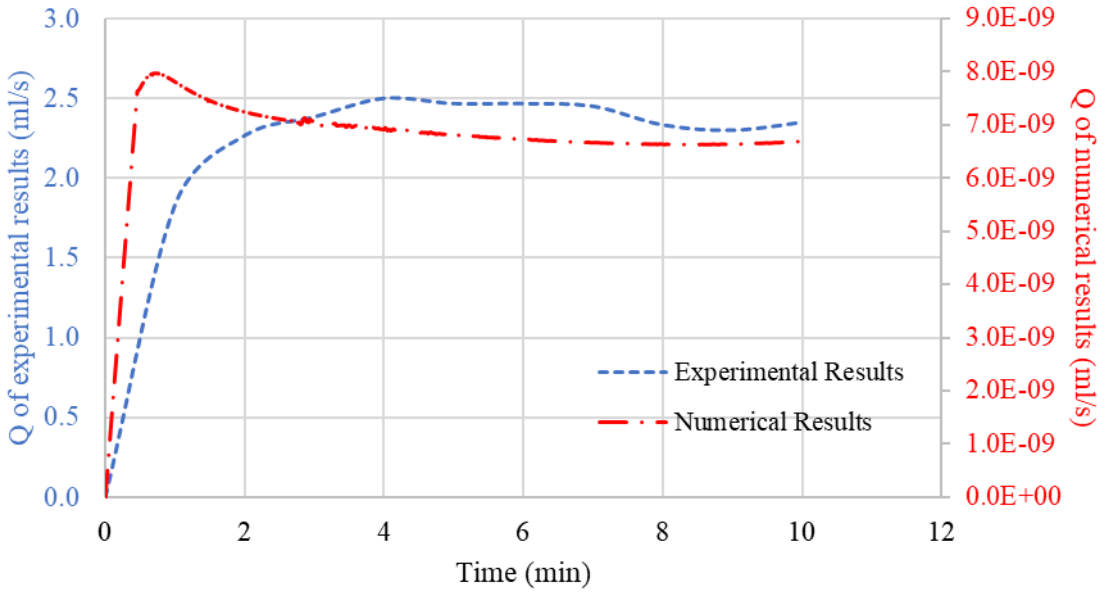

Figure 4.10 Comparison of outflow rates, Q of experimental (blue) and numerical (red) results for ST-2

4.5.3. Numerical Model Results of Static Test with 5% Fines Content in the Filter

Results of the static NEF test named ST-3 are given in detail in this section. The same unit system is valid for this test, too. Pore pressure distribution, discharge vectors, and hole displacement are shown in Figure 4.11a-c. The same pore water pressure (400 kPa) is applied to the inlet part of the model in a positive-y direction. ST-3 test duration is 11 minutes, so the numerical model is analyzed for 11 minutes.

The behavior of the water in this model is identical to ST-1 and ST-2. First, it goes through the gravel on the inlet side of the model; then, it reaches the hole which has the highest permeability in the model. After that, it follows through the filter and the gravel on the outlet side. The pore pressure distribution and displacement results are similar to ST-1 and ST-2 results. The discharge vectors have the smallest value among the tests. The outflow rate, Q, plot for both numerical model outcomes and experimental results is given in Figure 4.12.

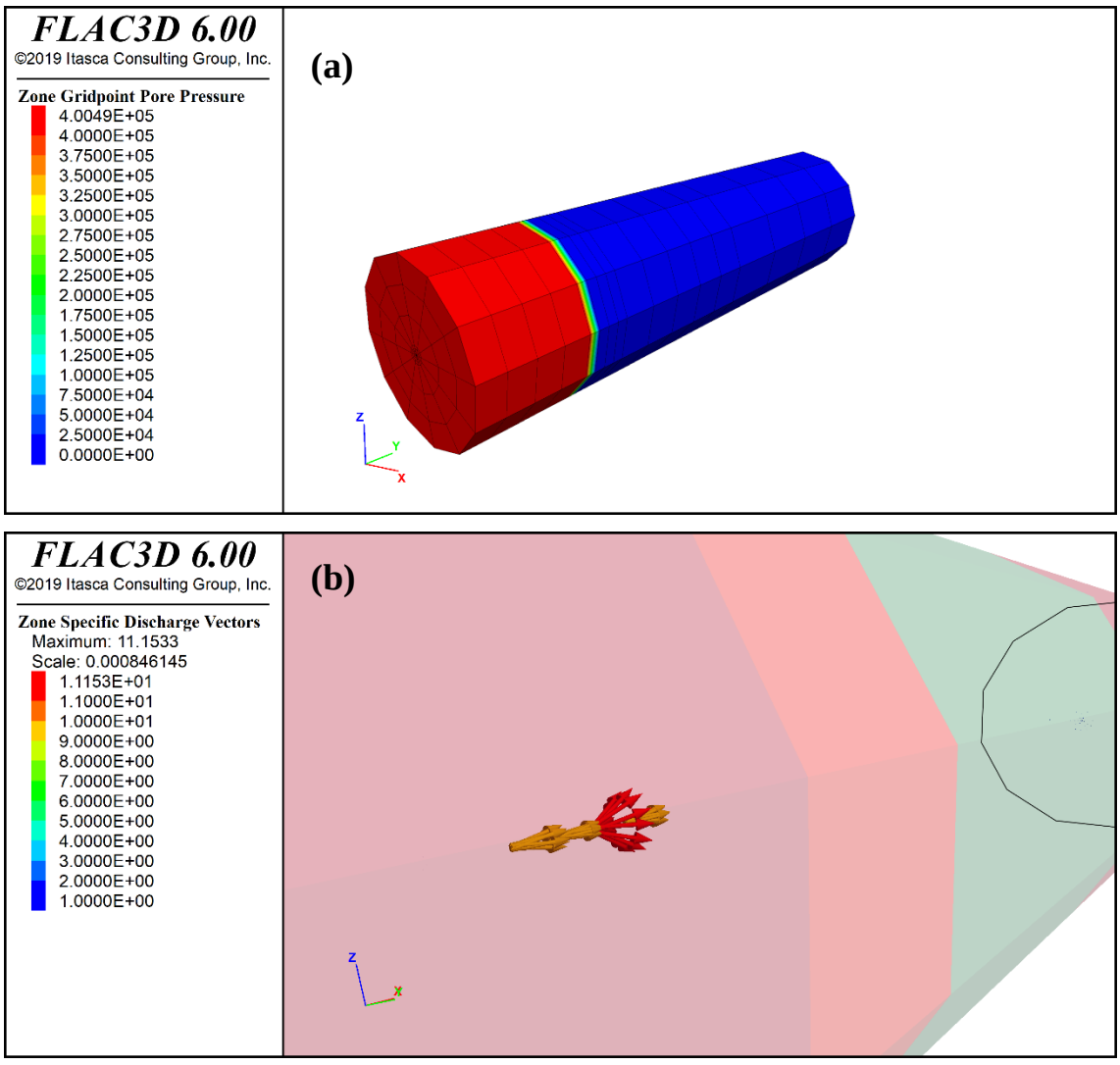

Figure 4.11 Numerical results of (a) Pore pressure distribution, (b) specific discharge vectors, (c) hole displacement vectors, of the static test with 5% fines content in the filter

(cont. on next page)

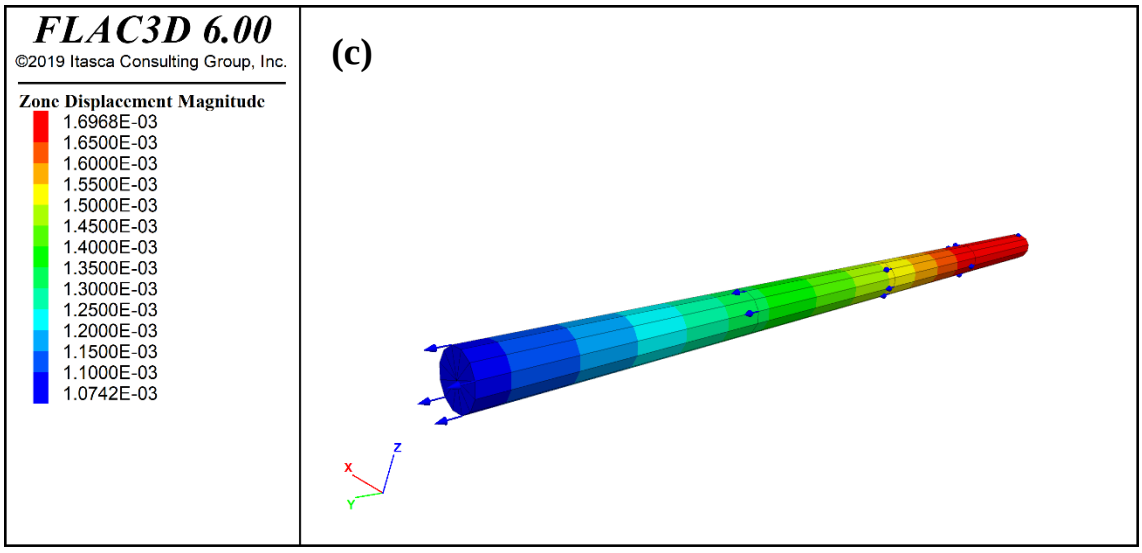

Figure 4.11 (cont.)

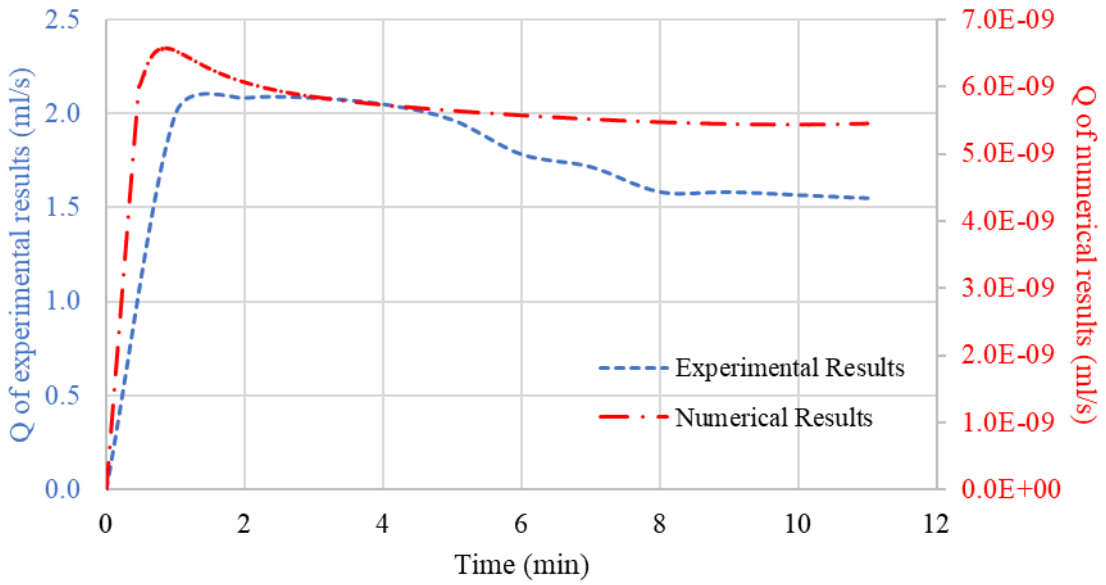

Figure 4.12 Comparison of outflow rates, Q of experimental (blue) and numerical (red) results for ST-3

4.5.4. Discussion on Numerical Results of Static Tests

The evaluations of the filters based on the laboratory tests, the clean filter sand is unsuccessful, and the others with 2% and 5% fine particles are successful (Table 3.5). The numerical model results of these tests are given in Figure 4.13a-b. However outflow rate of unsuccessful decreased and then stabilized after it saw the peak value in the laboratory tests (Figure 3.24a), it followed an increasing trend in numerical models when

the test was finished. Besides, in successful filters, the outflow rate reached a constant value in both tests and models.

Numerical results and experimental results of the outflow rate are plotted together in Figure 4.8, Figure 4.10, Figure 4.12 for each test (ST-1, ST-2, ST-3, respectively). It is seen that experimental results are 10^8-10^9 times bigger than the numerical results. The model does not give good agreement in the prediction of the outflow rate. When numerical models are compared to each other (Figure 4.13a), it is clear that the unsuccessful filter, which has 0% FC has a different behavior than successful filters, but the displacement behavior of successful and unsuccessful filters is identical. That's why it is thought that filter performance can be decided through the numerical model.

Specific discharge vectors are presented for each test in the previous sections. The maximum vectors are observed in the preformed hole. It is expected to see the highest discharge vectors in that region due to high hydraulic gradients based on the relationship given in the equation below (Robbins, 2016). Consequently, specific discharge values decrease in successful filters.

$$i = \frac{q_i}{k\rho_f g} \tag{4.5}$$

On the other hand, displacement values are relatively close to experimental results (Figure 4.13b). The final hole diameter in the unsuccessful test was 2 mm with a 1 mm increase. In numerical models, a 1 mm change in displacement was observed. However, the same increase is observed for successful filters.

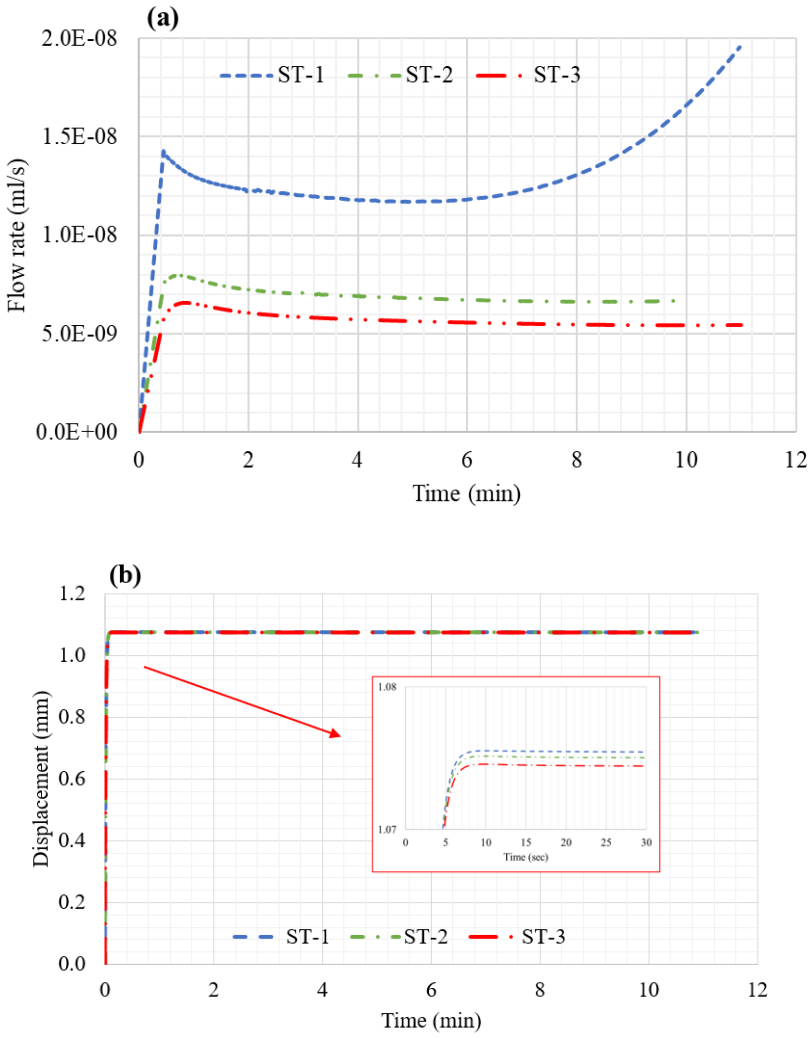

Figure 4.13 Numerical results of change in (a) outflow rate, and (b) displacement of the hole in the static tests over time

CHAPTER 5

PARAMETRIC STUDY ON NUMERICAL MODEL

5.1. Introduction

The previous chapter gives details on numerical models, and the comparison of outflow rate and displacement results of experimental and numerical results are presented. The comparison between numerical outcomes and experiments reveals that the flow rate of unsuccessful filters demonstrates different behavior than successful filters, whereas the displacement behavior is similar.

This chapter investigates the effect of the porosity of the base, permeability, and porosity of the filter on the outflow rate and displacement in the hole. The evaluations for filter performance were done to determine whether the outflow rate stabilized after 6 minutes or not. If the flow rate reaches a constant value, it is a successful test; however, if it shows an increasing trend, it is described as an unsuccessful test. Successful filters represent that the filter has the ability to mitigate internal erosion. It seals the crack in the base sample and does not let base particles to erode.

5.2. Effect of Porosity of the Base Material on Filter Performance

In this section, the influence of the porosity of the base material on internal erosion resistance is investigated. The maximum value of porosity for clay which is 0.70 (Hao et al., 2008), is taken in the analyses. As aforementioned, the Biot modulus and Biot coefficient have been changed with the porosity. The parameters used in the analysis and the original values used for the base are given in Table 5.1. The remaining parameters of the base are kept constant. The filter material properties are taken same as the parameters given in Table 4.2 and Table 4.3.

Table 5.1 Porosity, Biot modulus, and Biot coefficient used for the base material

$n_{original}$	n	$\alpha_{original}$	α	$M_{original}$ (Pa)	M (Pa)
0.32	0.70	0.41	0.78	107	49

It has been seen from the analysis results (Figure 5.1a) that increasing the base porosity generally raises the outflow rate in the first minutes of the test, and then it has the same values as the original porosity values. However, in an unsuccessful filter (ST-1) outflow rate at the end of the test is affected more, and increasing porosity causes a decrease in the outflow rate. On the other hand, the displacement rises with the porosity of the base (Figure 5.1b). However, it does not affect the filter performance at all. ST-1 is the unsuccessful filter, whereas ST-2 and ST-3 are the successful filters based on that the outflow rate remains at a constant value after 6 minutes.

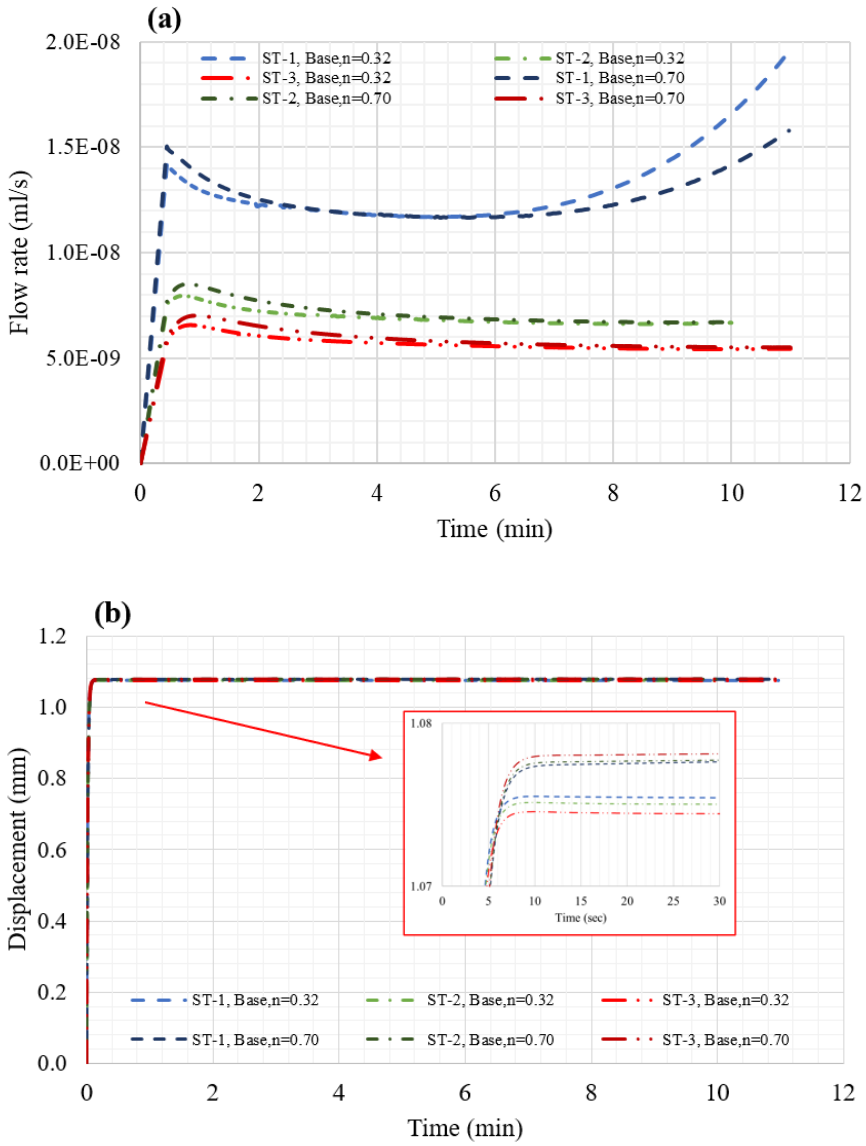

Figure 5.1 The effect of porosity of the base on change in (a) outflow rate, and (b) displacement of the hole, over time

5.3. Effect of Porosity of the Filter Material on Filter Performance

This section examines the influence of the porosity of the filter material on erosion behavior. Four sets of parametric studies (Filter #2, #3, #4, and #5) are performed to understand the influence of the filter's porosity. At first, the maximum value of the filter (sand) material in the literature is carried out. The remaining parameters of the filter materials are not changed in the analyses.

It is stated in the previous chapter that the Biot modulus and coefficient depend on the porosity value. Parameters (porosity, α, M) used in analyses to see the porosity effect are summarized in Table 5.2. Filter #1 (the original) represents the filter material that has no fine content. Flow rate and displacement results are demonstrated in Figure 5.2a-b.

Porosity change has affected the filter performance when investigating the flow rate and the displacement behavior of the unsuccessful test. As seen from Figure 5.2a, Filter #2 can be evaluated as successful due to the constant flow rate after the first 6 minutes of the test. However, the filter is already evaluated as unsuccessful in the laboratory and the numerical models. The flow rate decreases with the increase in filter porosity. It is unexpected because the transportation of base particles to the pores of the filter gets easier due to having more pores when porosity is higher. Erosion of the base particles causes higher flow rates and unsuccessful filters. Consequently, the porosity of the filter material may cause misevaluation for filter performance.

When the displacement values are compared, Filter #3 and Filter #5 have higher displacement values during the test. This is also unexpected because the porosity values of these filters are in the range of minimum and maximum values of porosity which are 0.260 and 0.50, respectively. However, maximum displacements are observed in the porosity of 0.40 and 0.35. Therefore, attention should be paid in the choice of porosity of the filter.

Table 5.2 Porosity, Biot modulus, and Biot coefficient used for the filter materials

Filter #	n	α	M (Pa)
1	0.26	0.35	132
2	0.50	0.60	68
3	0.40	0.50	86
4	0.30	0.39	114
5	0.35	0.45	98

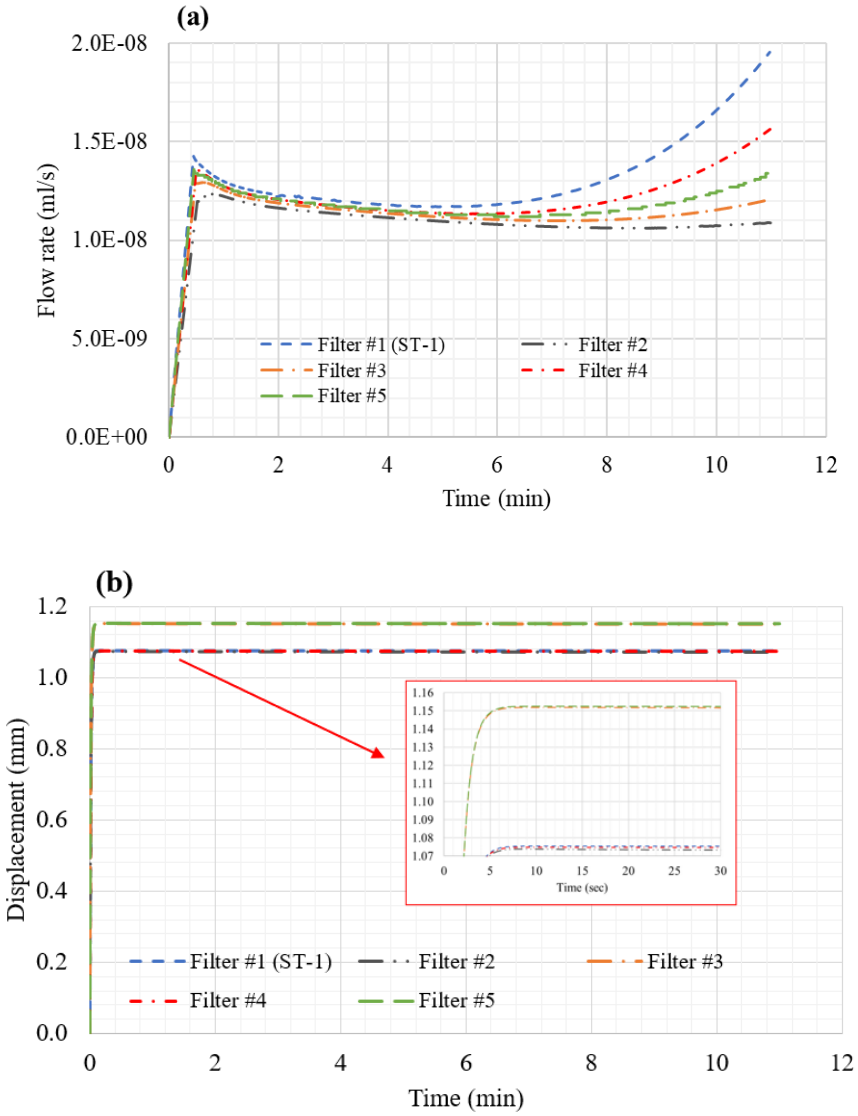

Figure 5.2 The effect of porosity of the filter on change in (a) outflow rate, (b) displacement of the hole, over time

5.4. Effect of Permeability of the Filter Material on Filter Performance

After the investigation of the porosity of the base and the filter materials, permeability influence on filter performance is examined. It is seen from Figure 4.13 that unsuccessful filter shows different outflow rate behavior rather than successful filters. By using this outcome, it is aimed to find the permeability values of the filter at which the behavior changes. After that, the maximum D_{10} value of the filter material that is not evaluated as unsuccessful is estimated. In the analyses, porosity values have not been changed due to that porosity affects outflow rate behavior. The permeability values used

in the analyses and their performances are summarized in Table 5.3. Filter #1 is the numerical results of the analyses using original test parameters (ST-1). The outflow rate and displacement results of the tests are demonstrated in Figure 5.3a-b.

The performance of the filters has been evaluated based on their flow rate trend, like Filter #1, which is the model results of the NEF test performed in the laboratory for the clean filter, which is decided as unsuccessful filter due to increasing flow rate after 6 minutes. Hereupon the performance of the filters has been examined, so Filter#4, Filter #6, and Filter #7 are found as successful. Filter #9 is also successful, which is already decided in the model of the NEF test for 5% fines content.

Eventually, the largest permeability among successful filters is around 0.0007 cm/s which belongs to Filter #4. By using this outcome and permeability correlations, the maximum D_{10} for a successful filter is suggested as 0.19 mm.

Table 5.3 Permeability values of filters and their performances

Filter #	k (cm/s)	Performance of the Filter
1	0.001120	**Unsuccessful**
2	0.000900	**Unsuccessful**
3	0.000800	**Unsuccessful**
4	0.000700	**Successful**
5	0.000750	**Unsuccessful**
6	0.000600	**Successful**
7	0.000650	**Successful**
8	0.000850	**Unsuccessful**
9	0.000523	**Successful**

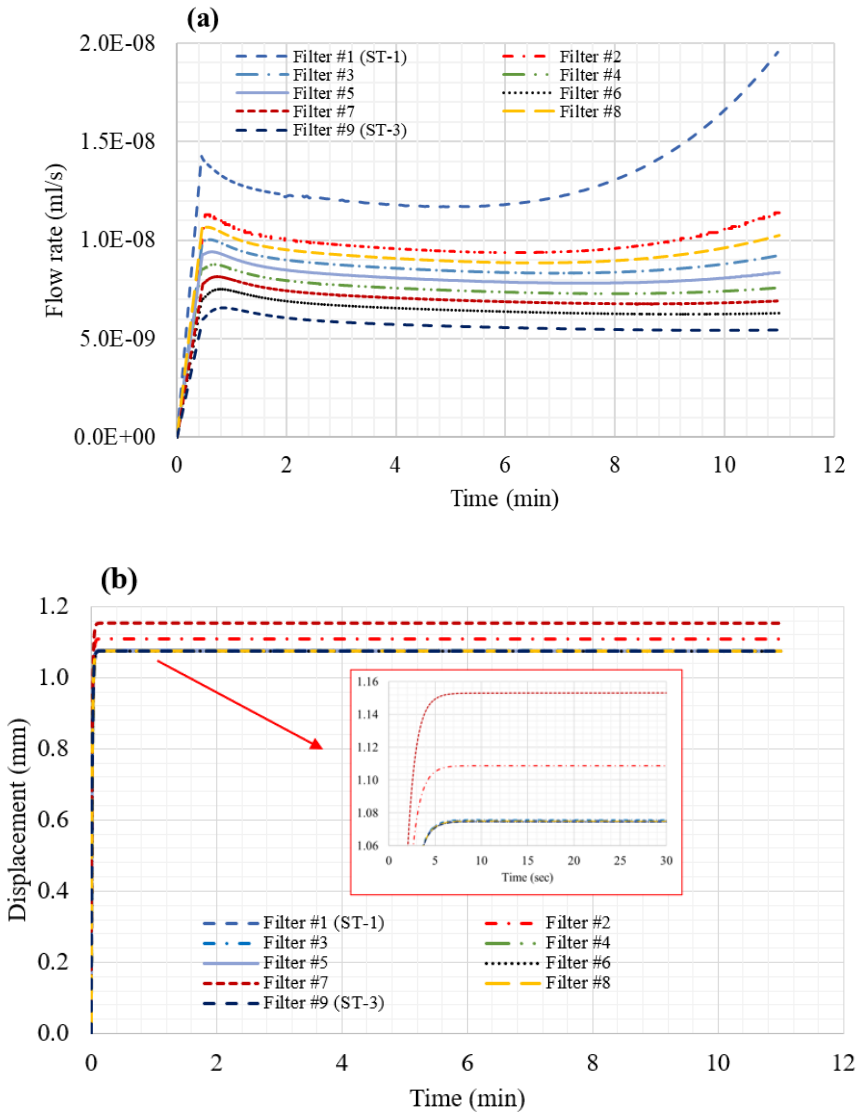

Figure 5.3 The effect of permeability of the filter on change in (a) outflow rate, and (b) displacement of the hole over time

5.5. Discussion on Parametric Study on Numerical Model

The NEF tests conducted in the scope of TUBITAK Project No. 221M071 (Ecemis, 2023) are simulated in FLAC3D. The outcomes of the numerical models are presented in CHAPTER 4. After verification and evaluation of the numerical study, parametric studies on the model are performed. The fundamental parameters that impact fluid flow through the model are porosity and permeability. For this reason, the porosity of the base and the filter; and the permeability value of the filter are chosen as the variables in the parametric study.

The results demonstrate that whereas the porosity of the base does not influence internal erosion, the porosity of the filter influences significantly. Based on the outcomes of the parametric study on the filter's porosity, porosity increase enhances resistance to internal erosion. However, the filter evaluated as unsuccessful in the experimental and numerical studies is found as successful in the parametric study. The choice of the filter's porosity is important in numerical modeling to avoid misevaluation. In addition to the parametric study of porosity, permeability influence is investigated, as well. The results show that internal erosion resistance increases with the decrease in the permeability value. Eight sets of parametric studies are performed to find a critical permeability value at which filter performance is changed from successful to unsuccessful or vice versa. The critical permeability is found as 0.0007 cm/s. The filters that have smaller permeability than this critical value are evaluated as successful. By using permeability correlations, the maximum D_{10} value in the gradation of filter sand is recommended as 0.19 mm. However, decreasing the permeability may affect seepage flow negatively, so the effective stresses increase. Therefore, soil stresses and the bearing capacity should be controlled.

In the next chapter, the thesis is concluded and summarized. All evaluations of numerical modeling of internal erosion through the NEF test are explained. Recommendations for future study are listed.

CHAPTER 6

CONCLUSION

In this chapter, the goal of the study, the NEF test data obtained from the TUBITAK Project No. 221M071 (Ecemis, 2023), methods for numerical modeling of internal erosion through the NEF test in finite difference environment, and the outcome of the study are summarized. Then, the recommendations for future works are mentioned.

6.1. Summary and Main Findings

As aforementioned, internal erosion is a serious threat to embankment dams which leads to progressive and catastrophic failure, so the understanding of this phenomenon is vital for dam safety (Foster et al., 2000). It can be prevented by using a protective filter; however, the design of the filter material should be proper both prevent erosion of the base material to its pores and should let water seepage through the dam body (Bonelli, 2013). Therefore, the complex behavior of individual particles and the water should be found out to design a proper filter.

The purpose of this study is to investigate the internal erosion by using finite difference approach through the NEF test conducted in the laboratory of IZTECH. Depending on this aim, Fast Lagrangian Analysis of Continua in a three-dimensional environment, FLAC3D 6.0 is used to model the NEF tests. After that, the parametric study on the numerical model is conducted.

In the scope of the TUBITAK Project, laboratory experiments on the samples were performed to obtain the physical properties of the samples before the NEF tests. Particle size distribution through sieve and hydrometer analyses, Atterberg limits, compaction of the base, and permeability of the filter were defined. Then, static and dynamic NEF test series were conducted on the filter and base samples of Kalabak Dam. Fines content and frequency were the variables of the tests for static and dynamic tests, respectively. The data for all the laboratory works were collected by Hadi Valizadeh in 2022 in the scope of TUBITAK Project No. 221M071 (Ecemis, 2023), and they are used for the verification of the numerical results in this study.

In numerical modeling, the data obtained for the filter and the base in the laboratory are defined. For gravel, average parameters in the literature are used, and for the hole, the parameters are taken as the largest permeability and porosity values and the smallest strength parameters based on analyses trials on FLAC3D. The outflow rate and the displacement of the preformed hole in the base samples were compared in the NEF tests and the numerical models. It is seen that the numerical results are 10^8-10^9 times smaller than the experimental results. However, the behavior of unsuccessful filter can be distinguished by showing different trend of outflow rate. Whereas it reaches a constant value in the experiments for all filters which have different fines content as 0%, 2% and 5%, it starts to raise after 6 minutes in numerical analyses. Xu et al. (2013) focused on concentrated leak erosion modeling, and they verified their results with Teton Dam by analytical approach and Excel VBA. The flow charge, which they calculated, increases over time in the piping process. Therefore, it has been decided to evaluate filter performance based on outflow rate behavior after 6 minutes in this study.

In addition to the outflow rate, displacement values of numerical results and experiments are compared. It is observed that displacement results in numerical models are close to each other for all tests. However, the displacement of the hole did not increase over time. It remained at a constant value in each test. The studies in the literature and the general concept of internal erosion include that the hole diameter keeps increasing over time (Mercier et al., 2014, Fujisawa et al., 2010). Even if the displacement vectors in the hole are in the same direction as the flow, the displacements may be caused by gravitational forces, as well.

Consequently, the performed NEF tests in the labotory has been modeled, and the effect of fines content on internal erosion has been investigated in numerical models in addition to laboratory tests. The unsuccessful filter which has no fine particles has been verified through the numerical study of static tests. Modeling of the dynamic series of the NEF tests are not performed in this study due to the boundary conditions problem. Present boundary conditions in FLAC3D, which are viscous and free-field, are not applicable to the model geometry (Itasca Consulting Group, Inc., 2017).

After modeling the experiments carried out in the laboratory of IZTECH, the parametric study is conducted by changing the porosity of the base and the filter and then the permeability of the filter. The outcomes of the parametric study reveal that the porosity of the base does not have a significant impact on the filter performance. On the other hand, the porosity of the filter may affect the performance of the filter. It shows

successful performance with the increase of the filter's porosity, so attention should be taken not to evaluate the filter incorrectly. The last part of the parametric study is the investigation of the permeability of the filter. Unsuccessful, which is the filter that has no fines content in the experiment series, is compared to the other filters with lower permeability values. To avoid the porosity effect in the numerical results, it is taken as the same as the original value, which is 0.26. It is seen that the maximum permeability of the filter is 0.0007 cm/s at which the filter demonstrates successful performance. It means that the filter that has higher permeability is unsuccessful. Eventually, by using correlations (Table 4.1), D_{10} value of the filter has been calculated as the maximum 0.19 mm of fine particles to show successful performance in internal erosion. In the design of filters, particle size distribution can be arranged based on this. However, it should be noted that when it gets smaller, the water flow through the filter gets harder, increasing excess pore water pressure.

To sum up, the NEF test is one of the main methods to design dam filters. It is practical and takes less time than other methods (Foster et al., 2001). Despite its advantages, numerical modeling is controversial because the parameters of the preformed hole inside the base sample are unpredictable, and it has a large computational burden caused by the huge difference in stiffnesses and permeability between the materials. Besides, the outflow rates of numerical results have not satisfied the experimental results. The difference between the experimental results and the numerical outcomes is around 10^8-10^9 times. Only the trend of outflow rate, Q, of the unsuccessful filter differs from the successful filters. Evaluations are made based on Q by considering increasing the flow rate after 6 minutes. Finally, the ability of FLAC3D in numerical modeling of concentrated leak erosion mechanism is doubtful based on this study. However, searching for the simulation of the concentrated leak erosion mechanism, which is a serious threat to embankment dams, is still required.

6.2. Recommendations for Future Research

In the literature, no study focuses on the numerical modeling of concentrated leak erosion mechanism and NEF Test by finite difference approach. In this study, the NEF test is modeled in FLAC3D 6.0, which uses finite difference method. However, the

complex behavior of soil and water together still needs to be searched, especially for concentrated leak erosion mechanism.

The numerical model does not have a good agreement with the experimental results. Even if so, filter performance is evaluated based on the outflow rate, as detailed in previous chapters. The recommendations for future research are listed below:

- Due to considerations in NEF test modeling, such as parameters of the hole and the boundary conditions, other methods CFD-DEM coupling, CFD only, or SPH can be preferred instead of FDM modeling.
- Current studies in the literature have considered the change in porosity and permeability in the eroded zone. The affected zone in the base material should be distinguished in future studies.
- The parametric study performed in this study shows that the porosity of the base material does not influence the filter performance. However, of the porosity of the filter investigation gives unexpected results, which may cause an incorrect evaluation of filter performance. Therefore, the effect of the filter's porosity should be investigated and decided carefully.
- Dynamic loading is not performed in this thesis study due to boundary problems in the model. In future research on the NEF test modeling, the boundary conditions should not affect the model performance.

REFERENCES

Bernatek-Jakiel, A., & Poesen, J. (2018). Subsurface erosion by soil piping: Significance and research needs. *Earth-Science Reviews*, *185*, 1107–1128. https://doi.org/10.1016/j.earscirev.2018.08.006

Bonelli Stéphane. (2013). *Erosion in geomechanics applied to dams and levees*. ISTE Ltd.

Cabalar, A. F., & Akbulut, N. (2016). Evaluation of actual and estimated hydraulic conductivity of sands with different gradation and shape. *SpringerPlus*, *5*(1). https://doi.org/10.1186/s40064-016-2472-2

Caldeira, L. (2018). Internal erosion in Dams. *Soils and Rocks*, *41*(3), 237–263. https://doi.org/10.28927/sr.413237

Chandel, A., & Shankar, V. (2021). Evaluation of empirical relationships to estimate the hydraulic conductivity of borehole soil samples. *ISH Journal of Hydraulic Engineering*, *28*(4), 368–377. https://doi.org/10.1080/09715010.2021.1902872

Cividini, A., & Gioda, G. (2004). Finite-element approach to the erosion and transport of fine particles in granular soils. *International Journal of Geomechanics*, *4*(3), 191–198. https://doi.org/10.1061/(asce)1532-3641(2004)4:3(191)

Dam Safety Office. (2004). *Evaluation of Protective Filter Erosion Boundaries* (Report No. DSO-04-04). Retrieved from Microsoft Word - Cover.doc (usbr.gov)

Delgado-Ramos, F., Poyatos, J. M., & Osorio, F. (2012). Internal erosion of clayey soils protected by granular filters. *La Houille Blanche*, *98*(4-5), 42–47. https://doi.org/10.1051/lhb/2012029

Ecemis, N. (2023). Dolgu Barajdaki Filter Kumunun Performansının Statik ve Dinamik Durumlarda Araştırılması. *1002 TUBITAK Project No. 221M071*.

Fanchi, J. R. (2010). *Integrated Reservoir Asset Management: Principles and best practices*. Gulf Professional Pub.

Fannin, J. (2008). Karl Terzaghi: From theory to practice in geotechnical filter design. *Journal of Geotechnical and Geoenvironmental Engineering*, *134*(3), 267–276. https://doi.org/10.1061/(asce)1090-0241(2008)134:3(267)

Fell, R., Patrick MacGregor, Stapledon, D., Bell, G., & Foster, M. (2014). *Geotechnical Engineering of Dams* (2nd ed.). CRC Press.

Fell, R., Wan, C. F., Cyganiewicz, J., & Foster, M. (2003). Time for development of internal erosion and piping in embankment dams. *Journal of Geotechnical and Geoenvironmental Engineering*, *129*(4), 307–314. https://doi.org/10.1061/(asce)1090-0241(2003)129:4(307)

FEMA. (2011). *Filters for Embankment Dams.* Federal Emergency Management Agency, Department of Homeland Security. Washington D.C., USA.

Foster, M., Fell, R., & Spannagle, M. (2000). The statistics of embankment dam failures and accidents. *Canadian Geotechnical Journal*, *37*(5), 1000–1024. https://doi.org/10.1139/t00-030

Fread, D. L.: BREACH, an erosion model for earthen dam failures, *Hydrol. Res. Laborat., National Weather Service, NOAA, Maryland, 1988.*

Frishfelds, V., Hellström, J. G., Lundström, T. S., & Mattsson, H. (2011). Fluid flow induced internal erosion within porous media: Modelling of the No Erosion Filter Test Experiment. *Transport in Porous Media*, *89*(3), 441–457. https://doi.org/10.1007/s11242-011-9779-9

Fry, J. (2016). Lessons on internal erosion in embankment dams from failures and physical models. *Scour and Erosion*. https://doi.org/10.1201/9781315375045-6

Graham P., and Wayne J. (1999) A procedure for estimating loss of life caused by dam failure. US Department of the Interior, Bureau of Reclamation, Dam Safety Office.

Hao, X., Ball, B. C., Culley, J. L. B., Carter, M. R., & Parkin, G. W. (2008). Soil density and porosity. *Soil sampling and methods of analysis*, 2, 179-196.

He, K., Song, C., & Fell, R. (2021). Numerical modelling of transverse cracking in embankment dams. *Computers and Geotechnics*, *132*, 104028. https://doi.org/10.1016/j.compgeo.2021.104028

I. Hellström J Gunnar. (2009). *Internal erosion in embankment dams: Fluid flow through and deformation of porous media*. Luleå University of Technology.

ICOLD. (1994). *Icold: Bull 95, 1994: Embankment dams granular filters and drains*.

Indraratna, B., Raut, A., & Locke, M. (2004). Granular filters in embankment dams: A conceptual overview and experimental investigation. *Geo Jordan 2004*. https://doi.org/10.1061/40735(143)2

International Commission on Large Dams. (2017). *Internal erosion of existing dams, levees and dikes, and their foundations = l'érosion interne dans les digues, barrages existants et leurs fondations*.

Itasca Consulting Group, Inc. (2016). *FLAC Version 8.1 Fast Langrangian Analysis of Continua.*

Itasca Consulting Group, Inc. (2017). *FLAC3D 6.0 Examples.*

Itasca Consulting Group, Inc. (2017). *FLAC3D 6.0 FLAC3D Modeling.*

Itasca Consulting Group, Inc. (2017). *FLAC3D 6.0 Theory and Background.*

Ma, G., Bui, H. H., Lian, Y., Tran, K. M., & Nguyen, G. D. (2022). A five-phase approach, SPH framework and applications for predictions of seepage-induced internal erosion and failure in unsaturated/saturated porous media. *Computer Methods in Applied Mechanics and Engineering*, *401*, 115614. https://doi.org/10.1016/j.cma.2022.115614

Mercier, F. (2014). *Numerical Modelling of Erosion of a Cohesive Soil by a Turbulent Flow* (thesis).

Mercier, F., Bonelli, S., Golay, F., Anselmet, F., Philippe, P., & Borghi, R. (2014). Numerical modelling of concentrated leak erosion during hole erosion tests. *Acta Geotechnica*, *10*(3), 319–332. https://doi.org/10.1007/s11440-014-0349-5

Molinder, G. (2016). Internal erosion in the pervious foundation of an embankment dam: A case study on the Lossen dam.

Newhouse, S. (2010). Earth dam failure by erosion: A case history. *Scour and Erosion*. https://doi.org/10.1061/41147(392)33

Nguyen, V.T. (2012). *Flow through filters in embankment dams*, Doctor of Philosophy thesis, School of Civil, Mining and Environmental Engineering, University of Wollongong.

Raeesosadat, A. R., Akhtarpour, A., & nazari, M. (2022). Filter Performance of Embankment Dams by No Erosion Filter Test (Case study: Bar and Bidvaz Dam). *Journal of Water and Sustainable Developement*, *8*(4), 69–76. https://doi.org/10.22067/JWSD.V8I4.2109.1077

Rahimi, M., & Shafieezadeh, A. (2020). Coupled backward erosion piping and slope instability performance model for levees. *Transportation Geotechnics, 24*, 100394. https://doi.org/10.1016/j.trgeo.2020.100394

Robbins, B. A., & Griffiths, D. V. (2018). Internal erosion of embankments: A review and appraisal. *Rocky Mountain Geo-Conference 2018*. https://doi.org/10.1061/9780784481936.005

Scheperboer, I. C., Suiker, A. S., Bosco, E., & Clemens, F. H. (2022). A coupled hydro-mechanical model for subsurface erosion with analyses of soil piping and Void Formation. *Acta Geotechnica, 17*(11), 4769–4798. https://doi.org/10.1007/s11440-022-01479-8

Sherard, J. L., & Dunnigan, L. P. (1989). Critical filters for impervious soils. *Journal of Geotechnical Engineering*, *115*(7), 927–947. https://doi.org/10.1061/(asce)0733-9410(1989)115:7(927)

Sherard, J. L., Dunnigan, L. P., & Talbot, J. R. (1984). Filters for silts and clays. *Journal of Geotechnical Engineering*, *110*(6), 701–718. https://doi.org/10.1061/(asce)0733-9410(1984)110:6(701)

State Hydraulic Works (Devlet Su İşleri, DSİ). (2006). *Regulation for Earthworks*.

State Hydraulic Works (Devlet Su İşleri, DSİ). *Regulation for Natural Construction Materials*.

Statistical analysis of failures of constructed embankment dams. (2016). *Dam Failure Mechanisms and Risk Assessment*, 11–24. https://doi.org/10.1002/9781118558522.ch2

Suits, L. D., Sheahan, T. C., Soroush, A., & Shourijeh, P. T. (2009). A review of the No Erosion Filter Test. *Geotechnical Testing Journal*, *32*(3), 101588. https://doi.org/10.1520/gtj101588

Sun, W., Fish, J., Liu, F., & Lu, Y. (2022). A stabilized two-phase pd-FEM coupling approach for modeling partially saturated porous media. *Acta Geotechnica*, *18*(2), 589–607. https://doi.org/10.1007/s11440-022-01619-0

Sun, Z., Tao, Y., Cao, Y., & Wang, Y. (2021). Numerical simulation of seepage failure of sandy soil between piles induced by an underground leaking pipe. *Arabian Journal for Science and Engineering*, *46*(11), 10489–10503. https://doi.org/10.1007/s13369-021-05354-8

Tabatabaie Shourijeh, P., Soroush, A., Shams Molavi, S., & Ramezani Fouladi, S. (2018). A parametric database study of no-erosion filter tests. *Proceedings of the Institution of Civil Engineers - Geotechnical Engineering*, *171*(3), 191–208. https://doi.org/10.1680/jgeen.17.00105

Tham, E. (2020). *On the use and interpretation of the Continuing Erosion Filter (CEF) test* (thesis).

Vahdati, P. (2014). *Identification of soil parameters in an embankment dam by mathematical optimization* (thesis). Luleå University of Technology, Luleå.

Vakili, A. H., Selamat, M. R., Mohajeri, P., & Moayedi, H. (2018). A critical review on filter design criteria for dispersive base soils. *Geotechnical and Geological Engineering*, *36*(4), 1933–1951. https://doi.org/10.1007/s10706-018-0453-7

Wan, C. F., & Fell, R. (2004). Investigation of rate of erosion of soils in embankment dams. *Journal of Geotechnical and Geoenvironmental Engineering*, *130*(4), 373–380. https://doi.org/10.1061/(asce)1090-0241(2004)130:4(373)

Wang, Y., Guo, N., Wang, S., & Gu, Y. (2016). Detection of internal erosion and piping in embankment dams. *Proceedings of the 2016 International Forum on Energy, Environment and Sustainable Development*. https://doi.org/10.2991/ifeesd-16.2016.21

Witt K. J. (1993) Reliability Study of Granular Filters, in *Filters in Geotechnical and Hydraulic Engineering, Geofilters 1992*, Brauns, Heibaum and Schuler, Eds., Balkema, Rotterdam, pp. 35–42.

Xu, T., & Zhang, L. (2013). Simulation of piping in earth dams due to concentrated leak erosion. *Geo-Congress 2013*. https://doi.org/10.1061/9780784412787.110

Zhang, L. M., Xu, Y., & Jia, J. S. (2009). Analysis of earth dam failures: A database approach. *Georisk: Assessment and Management of Risk for Engineered Systems and Geohazards*, *3*(3), 184–189. https://doi.org/10.1080/17499510902831759